FLAP-LAG-TORSION AEROELASTIC STABILITY OF A CIRCULATION CONTROL ROTOR IN FORWARD FLIGHT

INDERJIT CHOPRA and
CHANG-HO HONG
University of Maryland

ABSTRACT

The aeroelastic stability of a circulation control rotor blade undergoing three degrees of motion (flap, lag, and torsion) is investigated in forward flight. Quasi-steady strip theory is used to evaluate the aerodynamic forces; and the airfoil characteristics are from data tables. The propulsive and the auxiliary power trims are calculated from vehicle and rotor equilibrium equations through the numerical integration of element forces in azimuth as well as in radial directions. The nonlinear time dependent periodic blade response is calculated using an iterative procedure based on Floquet theory. The periodic perturbation equations are solved for stability using Floquet transition matrix theory. The effects of several parameters on blade stability are examined, including advance ratio, collective pitch, thrust level, shaft tilt, structural stiffnesses variation, and propulsive and auxiliary power trims.

INTRODUCTION

The airfoil on a circulation control (CC) rotor typically has quasi-elliptic profile and uses a tangential wall jet ejected over the rounded trailing edge to produce circulatory lift; (fig. 1). Due to the Coanda effect, the air remains attached at the rounded trailing edge and the stagnation point shifts to the lower surface. The lift of a CC airfoil can be controlled by jet momentum as well as by geometric incidence. It is possible to achieve high lift coefficients (four to five) with CC airfoils. Also, the aerodynamic center due to blowing circulation is near half-chord. For a general bibliography of circulation control see Englar and Applegate (1984). The application of CC technology to full-scale rotor design is currently being investigated (Linden and Biggers, 1985). The cyclic lift control of a CC rotor is obtained by a cyclic modulation of blowing. This eliminates the need for cyclic pitch and results in a simplified hub design. Collective lift control is obtained either by collective blowing or by collective pitch; see figure 2. Important features of a CC rotor are high thrust capability at reduced tip speeds and easy implementation of a higher harmonic control system. One area of concern, however, is the effect of CC aerodynamics on blade dynamics.

Johnson (1985) documented recent developments in the dynamics of advanced rotor systems. Few attempts have sbeen made to examine the aeroelastic stability of a CCR rotor blade (Chopra and Johnson, 1979; Chopra, 1984-85). An aeroelastic stability analysis of a CC rotor blade in hover was conducted by Chopra and Johnson in 1979. Three degrees of motion were considered: rigid flap, lag, and feather rotations about hinges at the blade root. The CC airfoil characteristics were represented in terms of analytical expressions. It was shown that the trailing edge blowing can have an important influence on blade dynamics and must, therefore, be addressed in rotor design. Chopra

---

*Work partially supported by David Taylor Naval Ship R & D Center under Contract No. N0016785-M-4464.
Presented at Circulation Control Workshop NASA Ames Research Center, February 1986.

(1984) also examined the aeroelastic stability of flap bending, lead-lag bending, and torsion of a CC rotor hingeless blade in hover using a finite element formulation. The CC airfoil characteristics were taken from data tables. Again, the stability results of hingeless rotors showed that the blowing has an important influence on blade dynamics. The finite element formulation was extended to analyze the aeroelastic stability of a bearingless rotor blade in hover (Chopra, 1985).

The objective of the present work is to examine the aeroelastic stability of a CC rotor blade in forward flight. For this, a simple flap-lag-torsion blade model consisting of three degrees of motion is considered. Quasi-steady strip theory is used to obtain aerodynamic forces. The effect of unsteady aerodynamics is introduced approximately through dynamic inflow modeling. The effects of pneumodynamics (Watkins et al., 1985) and centrifugal pumping in the pressure duct are included to calculate the jet momentum at a radial station.

The propulsive trim is calculated iteratively from the vehicle nonlinear equilibrium equations. Three force equations (vertical, longitudinal, and lateral) and two moment equations (pitch and roll) are obtained by numerically integrating the element forces both along the azimuth as well as the radial directions. The trim solution gives the rotor control setting and the vehicle orientation for a prescribed flight condition. The blade steady response is then calculated from nonlinear periodic blade equations using an iterative procedure based on Floquet theory. For stability, the blade motion is assumed to be a small perturbation about the steady response, and the linearized periodic blade equations are solved using Floquet transition matrix theory (Panda and Chopra, 1985). Stability results are calculated for typical CC rotor blades for several flight conditions.

FORMULATION

The blade is assumed to undergo three degrees of motion: rigid flap, lag, and feather rotations about hinges at the blade root, with hinge springs to obtain the desired natural frequencies. The hinge sequence is flap inboard, followed by lag, and then feather outboard. The flap angle β is positive up, the lag angle ζ is positive aft (opposite to rotation), and the feather angle θ is positive leading-edge up. The structural equations of motion include the inertial forces about three hinges and are documented by Panda and Chopra (1985). In general, terms up to second-order are retained in the flap and lag equations and terms up to third order are retained in the feather equation.

The aerodynamic forces are obtained using quasisteady strip theory. The section lift, drag, and moment about the mid-chord (per unit span) are

$$L = \frac{1}{2}\rho V^2 c C_\ell(\alpha, C_\mu)$$

$$D = \frac{1}{2}\rho V^2 c C_d(\alpha, C_\mu) \qquad (1)$$

$$M_{.5} = \frac{1}{2}\rho V^2 c^2 C_{m.5}(\alpha, C_\mu)$$

The aerodynamic coefficients C_ℓ, C_d, and $C_{m.5}$ are from data tables; the numerical values for these coefficients are available at small steps, $\Delta\alpha$ of 3 degrees and ΔC_μ of 1/200. These coefficients depend on the airfoil geometry, including slot height, and are also a function of angle of attack α, blowing momentum coefficient C_μ, and local Mach number. However, in the present work, the effect of compressibility (Mach number) is neglected. The C_μ is defined as

$$C_\mu = \frac{\dot{m}V_j^2}{qc} \tag{2}$$

where $\dot{m}V_j$ is the jet momentum, q (= 1/2 ρV^2) is the dynamic pressure, and c is the blade chord.

For an incompressible flow, using an isentropic expansion relationship, the momentum coefficient C_μ can be related to the local duct pressure P_d.

$$C_\mu = 2\frac{\bar{h}}{c}\frac{1}{q}(P_d - P_\infty) \tag{3}$$

where $\bar{h}/c$ is slot height-to-chord ratio (typically 0.002) and $P_d - P_\infty$ is duct gage pressure. The dynamic pressure at a radial station is

$$q = \frac{1}{2}\rho\,(\Omega R)^2\,(\frac{r}{R} + \mu\sin\psi)^2$$

For a compressible flow with a subsonic jet condition, the blowing momentum coefficient (Rogers et al., 1985) is

$$C_\mu = 2\frac{\bar{h}}{c}(M_j/M_\infty)^2 \quad \text{for} \quad (M_j < 1) \tag{4}$$

where M_j is the jet Mach number and M_∞ is free-stream Mach number. These relations, eqs. (3) and (4), for incompressible and compressible flows are valid only for the unchoked flow condition (when P_d/P_∞ is less than 1.892. For a P_d/P_∞ larger than 1.892, the flow becomes choked in the nozzle (slot). Then, the jet momentum coefficient is obtained as

$$C_\mu = \frac{2\frac{\bar{h}}{c}\frac{P_d}{P_\infty}M_j\,(\frac{2}{\gamma+1})^{\frac{\gamma+1}{2(\gamma-1)}}}{M_\infty^2\sqrt{1 + \frac{\gamma-1}{2}M_j^2}} \tag{5}$$

For both cases of unchoked and choked flows, the jet Mach number can be calculated in terms of duct pressure

$$M_j = \sqrt{5\left[\left(\frac{P_d}{P_\infty}\right)^{\frac{\gamma-1}{\gamma}} - 1\right]} \tag{6}$$

For an accurate representation of the blade internal duct pressure characteristics at an arbitrary local rotor disc location, pneumodynamic considerations are included in the analysis (Watkins et al., 1985). Between the duct pressure at a radial station and the cyclic pressure at the pneumatic valving system (blade root), there is a phase lag due to length, a pressure attenuation due to duct friction loss, and a pressure rise due to the centrifugal pumping effect. The duct pressure is obtained as

$$P_d = (P_{d_r} - P_\infty)\left\{1 - \eta_{duct}\left[\frac{r}{R} - \left(\frac{r}{R}\right)_{root}\right]\right\} + (P_{d_r}/P_\infty)\,\frac{\rho}{2}\left(\frac{r}{R}V_{tip}\right)^2 \eta_{pump} \tag{7}$$

and

$$P_{dr} = P_o + P_{1c}\cos(\psi - \phi) + P_{1s}\sin(\psi - \phi) \tag{8}$$

where ϕ is the phase lag for the pressure pulse at a radial station defined as

$$\phi = \frac{6\ rpm}{a_{duct}}(r - r_{root}) \quad deg \tag{9}$$

The term P_o is collective pressure, P_{1c} and P_{1s} are cyclic pressures at the blade root. The η_{duct} and η_{pump} are respectively the duct friction loss coefficient and the centrifugal pumping efficiency, respectively. The V_{tip} is tip speed (ΩR), r_{root} is root radius (where the pressure duct starts), P_∞ is atmospheric pressure (1827 lb/ft^2) and a_{duct} is speed of sound in the duct (1274 ft/sec).

Equations (7) through (9) show that the blowing momentum coefficient is a function of radial position r as well as azimuth angle ψ.

VEHICLE TRIM SOLUTION

Two types of trim solutions are considered corresponding to separate CC rotor aircraft concepts. The propulsive trim solution represents a CC rotor implemented in a conventional helicopter flight mode. There, the rotor produces all lift and propulsive forces. Alternatively, the constrained trim solution represents a CC rotor employed on a compound hleicopter configuration that also features auxiliary propulsive devices.

Propulsive Trim

The propulsive trim simulates the free flight condition. For specified weight

coefficient C_w, collective pitch θ_o, and forward speed μ, the trim solution calculates blowing settings (P_o, P_{1c} and P_{1s}), steady flap response (β_o, β_{1c}, and β_{1s}), vehicle orientation (α_s and ϕ_s) and steady inflow ratio λ.

The present propulsive trim is calculated from the satisfaction of three forces (vertical, horizontal and lateral) and two moments (pitch and roll) equilibrium equations. Figure 3 shows the forces and moments acting on the vehicle. The equilibrium equations have been defined by Panda and Chopra (1985).

For the vehicle trim solution, only the flap motion up to first harmonic is considered. Therefore, the following rotor equations are used.

$$\beta_o: \quad \frac{1}{2\pi}\int_o^{2\pi} (\text{flap equation})\, d\psi = 0 \tag{10}$$

$$\beta_{1c}: \quad \frac{1}{2\pi}\int_o^{2\pi} (\text{flap equation})\, \cos\psi\, d\psi = 0 \tag{11}$$

$$\beta_{1s}: \quad \frac{1}{2\pi}\int_o^{2\pi} (\text{flap equation})\, \sin\psi\, d\psi = 0 \tag{12}$$

For steady inflow, a linear distribution model developed by Drees is used,

$$\lambda = \mu \tan\alpha_s + \frac{1}{2}\,\frac{C_T}{\sqrt{\mu^2+\lambda^2}}\left(1 + K_x \frac{r}{R}\cos\psi + K_y \frac{r}{R}\sin\psi\right) \tag{13}$$

where

$$K_x = \frac{4}{3}\left[(1-1.8\mu^2)\sqrt{1+\left(\frac{\lambda}{\mu}\right)^2} - \frac{\lambda}{\mu}\right]$$

$$K_y = -2\mu$$

For hover, K_x and K_y become zero.

As stated earlier, the blowing momentum coefficient varies in both the radial as well as azimuth directions. Therefore, the aerodynamic coefficients (C_ℓ, C_d, and C_m) cannot be expressed in simple analytical expressions. To obtain the rotor coefficients (C_T, C_Y and C_H) for trim solution, the element forces must be integrated numerically in both the radial and the azimuth directions. Thus,

$$C_T = \frac{1}{4\pi(\Omega R)^2}\int_o^{2\pi}\int_o^{1} \sigma(x)\left(C_\ell \frac{U_T}{\Omega R}\frac{V}{\Omega R} - C_d \frac{U_P}{\Omega R}\frac{V}{\Omega R}\right) dx\, d\psi \tag{14}$$

$$C_H = \frac{1}{4\pi(\Omega R)^2} \int_0^{2\pi} \int_0^1 \sigma(x) \left[\left(C_\ell \frac{U_P}{\Omega R} \frac{V}{\Omega R} + C_d \frac{U_T}{\Omega R} \frac{V}{\Omega R} \right) \sin\psi \right.$$

$$\left. + \left(C_d \frac{U_R}{\Omega R} \frac{V}{\Omega R} - \beta\, C_\ell \frac{V}{\Omega R} \frac{V}{\Omega R} \right) \cos\psi \right] dx\, d\psi \qquad (15)$$

$$C_Y = \frac{1}{4\pi(\Omega R)^2} \int_0^{2\pi} \int_0^1 \sigma(x) \left[-\left(C_\ell \frac{U_P}{\Omega R} \frac{V}{\Omega R} + C_d \frac{U_T}{\Omega R} \frac{V}{\Omega R} \right) \cos\psi \right.$$

$$\left. + \left(C_d \frac{U_R}{\Omega R} \frac{V}{\Omega R} - \beta\, C_\ell \frac{V}{\Omega R} \frac{V}{\Omega R} \right) \sin\psi \right] dx\, d\psi$$

where U_P, U_T, U_R and V are section flow velocity components; see figure 4. The x is the nondimensional coordinate r/R, and $\sigma(x)$ is the local solidity ratio.

The vehicle and rotor equilibrium equations are obtained for large angles. These equations which are expressed in nondimensional form, are presented in the appendix. The nonlinear equations are solved iteratively for the trim solution using the Newton-Raphson procedure.

CONSTRAINED TRIM

The constrained trim solution, where propulsive force is partially obtained from auxiliary power, is calculated by satisfying the vertical force, pitch moment, and roll moment equilibrium equations. The vehicle orientation is specified in terms of shaft tilt α_s; lateral tilt ϕ_s is zero. Since the trim solution is for an isolated rotor, the characteristics of the vehicle are not needed. For the specified weight coefficient C_W, collective pitch θ_o, and advance ratio μ, the trim solution calculates blowing settings (P_o, P_{1c} and P_{1s}) and rotor response (β_o, β_{1c} and β_{1s}). This solution procedure is similar to that used in the propulsive trim solution.

Alternative constrained trim procedure is to fix the collective blowing pressure (e.g. $P_o = 1.5\ P_\infty$) and adjust the collective geometric pitch to obtain the desired thrust level. This trim procedure though not implemented in the present work, would yield equivalent blade stability results.

BLADE RESPONSE SOLUTION

The blade response solution involves the determination of the time dependent blade deflected position. For steady flight conditions, the blade response is periodic, and hence the solution is calculated for only one complete cycle. For this, the nonlinear coupled blade equations containing periodic terms are solved in the rotating frame using an iterative procedure based on Floquet theory (Dugundji and Wendell, 1983). For the blade response solution, the pilot controls and the vehicle orientation obtained from

the trim solution are used. The numerical procedure to calculate the initial conditions and the blade response along the azimuth are detailed by Panda and Chopra (1985). The calculated response solution consists of all harmonics for flap, lag, and torsion motions.

It should be noted that there is another cycle of iterations (typically two) between the trim solution and the blade response solution to include the effect of blade elastic twist in the trim calculations.

STABILITY SOLUTIONS

The stability of blade perturbation motion about its steady deflected position is examined using the vehicle trim and the blade response solutions. For perturbation motion, unsteady aerodynamic effects are introduced approximately through a dynamic inflow modeling. The dynamic inflow is assumed to be a perturbation about the steady value, and its components are related to rotor perturbation forces and moments (Panda and Chopra, 1985).

The blade perturbation equations are transformed to the fixed reference frame using Fourier coordinate transformation. These equations, which contain selected harmonic terms, are solved for stability using Floquet transition matrix theory.

RESULTS AND DISCUSSION

Numerical results are calculated for a four-bladed CC rotor with Lock number $\gamma = 5$, solidity ratio $\sigma = 0.13$, and zero precone. The blade flap, lag and torsion rotating frequencies are 2.3/rev, 2.6/rev and 18/rev, respectively. The chordwise offsets of the center of mass and the reference aerodynamic center from the elastic axis are considered to be zero, and the elastic axis is assumed to be at the midchord position. For stability calculations, the structural damping is assumed to be zero for all modes. For airfoil characteristics, tabular data of a typical CC airfoil with trailing edge blowing (single slot) is used. Other rotor and vehicle characteristics are given in table I.

PROPULSIVE TRIM

Numerical results are calculated for $C_w/\sigma = 0.1$. Figure 5 shows the vehicle propulsive trim solution for a collective pitch of zero. The propulsive trim parameters P_o, P_{1C}, P_{1S}, α_S, ϕ_S, and λ are plotted for different forward speeds (in terms of advance ratio μ). An advance ratio of 0.6 represents a forward speed of about 300 ft/sec and a maximum tip speed of 850 ft/sec. The root blowing pressures, collective (P_o) and cyclic (P_{1C} and P_{1S}), are presented in terms of atmospheric pressure (P_∞). The flap angles (β_o, β_{1C} and β_{1S}) are negligible for this highly stiff rotor and hence are not presented. The trim solution is calculated iteratively from nonlinear equilibruim equations. As conventional rotor, the shaft has to tilt more forward at larger μ in order to compensate for the increasing parasite drag. The inflow λ first decreases and then increases with forward speed due to the combined effect of decreasing induced velocity and increasing disk tilt (α_S) at larger μ. There is only a slight influence of μ on side shaft tilt ϕ_S. The collective and cyclic blowing pressure requirements with advance ratio μ appear quite similar to the respective geometric pitch requirements of a

conventional rotor (Panda and Chopra, 1985). The cyclic blowing pressures (P_{1C} and P_{1S}) are much smaller than the collective blowing pressure (P_0). The periodic variation of dynamic pressure is compensated for by the cyclic blowing components. At low forward speeds both P_{1C} and P_{1S} are of equal importance because of the nonuniform induced velocity; however at higher speeds, P_{1S} becomes larger than P_{1C}.

TABLE I - CCR Rotor Characteristics in Analysis

Rotor radius R	28.5 ft
Tip speed ΩR	500 ft/sec
Chord-to-radius ratio, c/R	0.1
Airfoil thickness ratio, t/c	0.15
Slot height-to-chord ratio, $\bar{h}$	0.002
Feather inertia-to-flap inertia ratio, I_f/I_b	0.0024
Reference lift curve slope, a	5.7
Vertical cg offset from hub, h	0.2R
Duct speed of sound a_{duct}	1274 ft/sec
Duct friction loss coefficient, η_{duct}	0.15
Centrifugal pumping efficiency, η_{pump}	0.57
Root radius-to-rotor radius ratio, $(r/R)_{root}$	0.1

A word of caution: these and subsequent results are calculated using the linear inflow model of Drees, which perhaps underestimates the longitudinal inflow variation at low forward speeds ($\mu < 0.15$). In addition, blowing in the reversed flow regions is assumed to produce no circulatory lift.

Figure 6 presents the propulsive trim solution for a collective pitch of -10 degrees. For this pitch setting, a larger collective blowing pressure is needed to achieve the prescribed thrust level. With this negative collective pitch, there are changes on other trim parameters (λ, α_s, and ϕ_s); in fact, their values become almost double those of zero pitch. Trim results without pneumodynamic effects (pressure loss, phase lag, and centrifugal pumping) are shown in figure 6(b). There is a small step decrease in collective blowing pressure for all forward speeds because of reduced losses. Neglecting pneumodynamics in the calculations also influences cyclic pressures; P_{1S} decreases and P_{1C} increases.

In figure 7, the time-dependent position of the blade is presented for one complete cycle. The blade is set at zero collective pitch, and the propulsive trim solution is employed. These results are obtained by solving the nonlinear periodic equations using an iterative procedure based on Floquet theory. For numerical integration, a fourth-order Runge-Kutta method and 240 time steps per cycle ($\Delta\psi$ = 1.5 degrees) are used. The blade is extremely stiff in flap mode (flap frequency = 2.3/rev) and, therefore, a small flap response is expected. At a low forward speed (μ = 0.2), there is a very little flap response. However, at high forward speeds, the flap response becomes greater induced by a larger variation in aerodynamic environment along the azimuth. At μ = 0.4, the flap response consists primarily of the second harmonic with a maximum peak-to-peak amplitude of about 0.75 degrees. At high μ of 0.6, the flap response is again dominated by a 2/rev component with a maximum peak-to-peak amplitude of about 2.5 degrees, which is perhaps a large flap response for this highly stiff rotor.

Figure 8 shows the damping of the low frequency cyclic lag mode for different advance ratios and collective pitch. Results are obtained from the eigen solution of Floquet transition matrix. Again, for the stability solution, 240 time steps per cycle are used for time integration. The eigenvalues represent rotor frequencies in the fixed reference frame. For this case, the low frequency lag mode is a regressive mode. The damping is presented in terms of the real part of the complex eigenvalue, α_ζ. Note that $\alpha_\zeta = \zeta_L \omega_\zeta$, where ζ_L is the viscous damping ratio of the lag mode, and ω_ζ is the frequency of lag mode nondimensionalized with respect to rotational speed. For the case of zero collective pitch, the blade is stable but the damping level in lag damping is quite low. However, the inclusion of structural damping will increase blade stability. In addition, negative collective pitch also has a stabilizing influence on lag mode. It is interesting to note that the variation of forward speed has only a slight influence on lag damping.

Figures 9 through 11 show the effect of thrust level on blade lag mode stability. For a fixed-collective pitch, the rotor thrust level is a near linear function of blowing pressure. Using the previous thrust coefficient of C_T/σ of 0.1. as a reference, three additional thrust levels are considered: C_T/σ = 0.05, 0.15, and 0.2. Figure 9 presents the lag mode damping for zero collective pitch. In general, the reduced thrust level stabilzes lag mode at low forward speeds and destabililizes lag mode at high forward speeds. For C_T/σ = 0.15, lag mode is unstable for $\mu < 0.15$, whereas, for C_T/σ = 0.05, lag mode is unstable for $\mu > 0.41$. This observed instability is quite weak in nature and can be easily stabilized with the inclusion of a small amount of structural damping in lag mode. In Figure 10, somewhat similar results are seen for a collective pitch of -5 degrees. For a low thrust level condition of C_T/σ = 0.05, the lag mode becomes unstable for $\mu > 0.42$. At this thrust level, the solution is not obtained for $\mu > 0.51$. The lateral cyclic blowing component becomes larger than the collectiv blowing level; therefore, P_{root} becomes less than P_∞ locally on the advancing side of the rotor. Again the damping requirements to stabilize the lag mode are not high, and the expected levels of internal structural damping would ensure this stability. Figure 11 shows lag mode damping for a collective pitch of -10 degrees. With this high negative pitch, the lag mode damping generally becomes more stable. The exception is C_T/σ = 0.2, for which the blade lag mode becomes less stable at high forward speeds.

Figure 12 shows the effect of torsional stiffness on lag mode stability. The earlier results are for a rotating torsional frequency of 18/rev. Figure 12(a) presents results for zero collective pitch. If the torsion frequency is reduced to 10/rev, there is only a slight effect on lag mode damping. A further reduction in torsional stiffness

has an appreciable effect on lag mode stability. For a torsional frequency of 5/rev, the lag mode becomes unstable and the instability increases at high advance ratios. In figure 12(b), results are presented for a collective pitch of -10 degrees. Again, reducing torsional stiffness decreases lag mode damping.

The effect of lag stiffness on lag mode damping is presented in figure 13. The earlier results are for a rotating lag frequency of 2.6/rev. As compared with conventional rotors, this is a case of extremely high lag stiffness. For zero collective pitch, figure 13(a), if the lag frequency is reduced to the level of a typical stiff-inplane hingeless rotor ($\nu_\zeta = 1.4$), the lag damping is only slightly reduced. If the lag damping is further reduced to the level of a typical soft-inplane rotor ($\nu_\zeta = 0.7$), again the effect on lag damping again is quite negligible. For a negative collective pitch of 10 degrees figure 13(b), the effect of reducing lag stiffness to the conventional rotor value is quite destabilizing.

Figure 14 presents the effect of flap stiffness on lag mode damping. The earlier results are obtained for a rotating flap frequency of 2.3/rev. In comparing with the existing rotors, this is an extremely high flap stiffness. For zero collective pitch figure 14(a), if the flap frequency is reduced to 1.5/rev (level of ABC Rotor), the lag mode becomes slightly more stable, and even more so at high advance ratios. If the flap frequency is further reduced to 1.1/rev, to the level of a typical hingeless rotor(e.g. BO-105), the lag mode becomes unstable at high advance ratios ($\mu > 0.48$). For a collective pitch of -10 degrees Figure 14(b), the trends of lag mode damping with decreasing flap stiffness are somewhat different. The blade, however, remains stable.

Figure 15 shows the effect of pneumodynamics on lag mode damping. The blade is set at a collective pitch of -10 degrees. Neglecting pneumodynamics effects reduces lag mode damping slightly.

CONSTRAINED TRIM

Constrained trim calculates rotor controls to achieve a desired thrust and shaft orientation. This type of trim condition is possible through an auxiliary propulsive device. The solution is obtained by satisfying three rotor equilibrium equations (vertical force, pitch moment, and roll moment). This is an isolated rotor trim solution, and the airframe characteristics are not needed. With an auxiliary propulsive device, it is possible to achieve high forward speeds without causing excessive shaft tilts. Thus, the subsequent results using constrained trim include a larger range of advance ratios (up to 1.0). An advance ratio of 1.0 represents a forward speed of about 500 ft/sec and a maximum tip speed of 1000 ft/sec. The compressibility effects, however, have not been considered in the present work.

The constrained trim solution for zero collective pitch and zero shaft angle is shown in figure 16. The collective and cyclic components of blowing pressure at blade root are quite similar to those obtained with propulsive trim for zero collective pitch; Figure 5. The collective pressure P_o is somewhat smaller at higher advance ratios because of reduced inflow through the disk. For $\mu > 0.41$, the solution is not practical because of the pressure constraint ($P_{root} < P_\infty$). In figure 17, the constraint trim solution is presented for zero shaft angle and a collective pitch of -5 degrees. Once again, the collective pressure requirements at high μ are comparatively smaller than those of the propulsive rotor.

Figure 18 presents the blade flap response for one complete cycle. For this cycle, the rotor is set at zero shaft angle and zero collective pitch. For a low advance ratio ($\mu = 0.2$), the flap response amplitude is small. At high advance ratios, there is considerable flap response, consisting primarily of a 2/rev component. For $\mu = 0.5$, the peak-to-peak amplitude is about 1 degrees, whereas, for $\mu = 1.0$, the peak-to-peak amplitude is about 3.5 degrees.

Figure 19 shows the lag mode stability results for zero shaft angle. The lag mode is less damped for zero collective pitch. The negative collective pitch stabilizes lag mode damping. For collective pitch of 0 degrees the results are discontinued for μ larger than 0.42 because of the blowing pressure constraint ($P_{root} < P_{\infty}$).

In figure 20, the lag mode damping results are presented for a shaft angle of 5 degrees. This is a forward tilt of rotor shaft and the inflow through the rotor disk increases, resulting in an increased collective pressure requirement. Compared with results obtained for zero shaft angle (Fig. 19), the lag mode is slightly less stable for both cases of collective pitch. Note that the zero collective case can now be extended up to an advance of 1.0.

Figure 21 shows lag mode stability results for a shaft angle of -5 degrees. This is a rearward tilt of rotor shaft, and the inflow through the rotor disk decreases, resulting in a decreased collective pressure requirement. Compared with results obtained for zero shaft angle (Fig. 19) the lag mode is more stable for both cases of collective pitch. With the reduced collective pressure the range of μ for zero collective pitch is now reduced to 0.31.

CONCLUSIONS

Aeroelastic stability of a simple, three-degree-of-freedom (flap-lag-torsion) CCR blade model in forward flight is examined. Results are obtained using propulsive trim as well as auxiliary power trim. Based on the results of this study, the following conclusions are drawn.

Flap response consists primarily of 2/rev, and its amplitude increases with μ (peak-to-peak amplitude of 2.5 degrees at $\mu = 0.6$ for propulsive rotor)

Lag mode damping becomes more stable as collective pitch is decreased.

At high forward speeds ($\mu > 0.4$), lag mode becomes unstable at low thrust levels ($C_T/\sigma = .05$).

Reducing the stiffness of a highly stiff CC rotor blade to the level of a typical hingeless blade can cause lag mode instability.

The results obtained with auxiliary power trim are quite similar to those obtained with propulsive trim.

REFERENCES

Chopra, I.: Aeroelastic Stability of an Elastic Circulation Control Rotor Blade in Hover. Vertica, Vol. 8, No. 4, Oct 1984.

Chopra, I.: Dynamic Stability of a Bearingless Circulation Control Rotor Blade in Hover. Journal of the American Helicopter Society, Vol. 30, No. 4, Oct 1985.

Chopra, I. and Johnson, W.: Flap-lag-torsion Aeroelastic Stability of Circulation-Controlled Rotors in Hover. Journal of the American Helicopter Society, Vol. 24, No. 2, Apr 1979.

Dugundji, J. and Wendell, H.: Some Analysis Methods for Rotating Systems with Periodic Coefficients. AIAA Journal, Vol. 21, No. 6, Jun 1983.

Englar, R.J. and Applegate, C.A.: Circulation Control - A Bibliography of DTNSRDC Research and Selected Outside References. David W. Taylor Research and Development Center Report DTNSRDC-84/052, Sep 1984.

Johnson, W.: Recent Developments in the Dynamics of Advanced Rotor Systems. NASA TM 86669, Mar 1985.

Linden, A.W. and Biggers, J.C.: X-Wing Potential for Navy Applications. Paper presented at 41st Annual Forum of American Helicopter Society, Fort Worth, Texas, 15-17 May 1985.

Panda B. and Chopra I.: Flap-lag-torsion Stability in Forward Flight. Journal of the American Helicopter Society, Vol. 30, No. 4, Oct 1985.

Rogers, E.O., Schwartz, A.W. and Abramson, J.S.: Applied Aerodynamics of Circulation Control Airfoils and Rotors. Paper presented at 41st Annual Forum of the American Helicopter Society, Fort Worth, Texas, May 1985.

Watkins, C.B., Reader, K.R. and Dutta, S.K.: Pneumodynamic Characteristics of a Circulation Control Rotor Model. Journal of the American Helicopter Society, Vol. 30, No. 3, Jul 1985.

Appendix

Nonlinear Equations for Trim Solution

$$F(1) = \frac{-(\nu_\beta^2-1)/\gamma}{2\,\frac{h}{R}\,C_T/\sigma a}\,\beta_{1C} - X_{cg}/h\,\cos\alpha_s + \sin\alpha_s - \frac{1}{2}\,\mu^2\,\frac{f}{A}\,\frac{1}{C_w}$$

$$(\cos\alpha_s - \frac{X_{cg}}{h}\sin\alpha_s) + \frac{M_{yF}}{hW} \qquad \text{(Pitch moment)}$$

$$F(2) = 1 - \frac{C_T}{C_w}\cos\phi_s\,\cos\alpha_s - \frac{C_H}{C_w}\sin\alpha_s + \frac{C_Y}{C_w}\sin\phi_s$$

$$+ \frac{C_{YF}}{C_w}\sin\phi_s + \frac{1}{2}\,\mu^2\,\frac{f}{A}\,\frac{1}{C_w}\sin\phi_s \qquad \text{(Vertical force)}$$

$$F(3) = \frac{1}{2}\,\mu^2\,\frac{f}{A}\,\frac{1}{C_w} + \frac{C_H}{C_w}\cos\alpha_s - \frac{C_T}{C_w}\sin\alpha_s\,\cos\phi_s \qquad \text{(Longitudinal force)}$$

$$F(4) = (\frac{C_{YF}}{C_w} + \frac{C_Y)}{C_w}\cos\phi_s + \frac{C_T}{C_w}\sin\phi_s\,\cos\alpha_s \qquad \text{(Lateral force)}$$

$$F(5) = \frac{-(\nu_\beta^2-1)/\gamma}{2\,\frac{h}{R}\,C_T/\sigma a}\,\beta_{1s} + (\cos\phi_s + \frac{Y_{cg}}{h}\sin\phi_s)\,\frac{C_{YF}}{C_w}$$

$$+ \sin\phi_s - \frac{Y_{cg}}{h}\cos\phi_s + \frac{M_{xF}}{hW} \qquad \text{(Roll moment)}$$

$$F(6) = \lambda - \mu\,\tan\alpha_s - \frac{C_w}{2}\,\frac{1}{\sqrt{\mu^2+\lambda^2}}\,(1 + K_x\,\frac{r}{R}\cos\psi + K_y\,\frac{r}{R}\sin\psi) \qquad \text{(Inflow)}$$

$$F(7) = \beta_o - \frac{1}{4\pi}\,\frac{\gamma}{\nu_\beta^2}\int_o^{2\pi}\int_o^1 x\,V^2 C_\ell\,dx\,d\psi \qquad \text{(Flap } \beta_o\text{)}$$

$$F(8) = \beta_{1C} - \frac{1}{4\pi} \frac{\gamma}{(\nu_\beta^2 - 1)} \int_0^{2\pi} \int_0^1 x V^2 C_\ell \cos\psi \, dx \, d\psi \qquad \text{(Flap } \beta_{1C}\text{)}$$

$$F(9) = \beta_{1S} - \frac{1}{4\pi} \frac{\gamma}{(\nu_\beta^2 - 1)} \int_0^{2\pi} \int_0^1 x V^2 C_\ell \sin\psi \, dx \, d\psi \qquad \text{(Flap } \beta_{1S}\text{)}$$

$$F(10) = \frac{C_T}{C_w} - \frac{a}{4\pi} \frac{1}{C_w} \int_0^{2\pi} \int_0^1 \sigma U_T V C_\ell \, dx \, d\psi \qquad \text{(Rotor thrust)}$$

$$F(11) = \frac{C_H}{C_w} - \frac{a}{4\pi} \frac{1}{C_w} \int_0^{2\pi} \int_0^1 \sigma \left[U_P V C_\ell + U_T V C_d \right) \sin\psi$$

$$+ \left(U_R V C_d - V^2 \beta C_\ell \right) \cos\psi \Big] \, dx \, d\psi \qquad \text{(Rotor drag)}$$

$$F(12) = \frac{C_Y}{C_w} - \frac{a}{4\pi} \frac{1}{C_w} \int_0^{2\pi} \int_0^1 \sigma \left[-(U_P V C_\ell + U_T V C_d) \cos\psi \right.$$

$$\left. + (U_R V C_d - V^2 \beta C_\ell) \sin\psi \right] dx \, d\psi \qquad \text{(Rotor side force)}$$

In the expressions, the flow components U_P, U_T, and V are nondimensionalized with respect to ΩR.

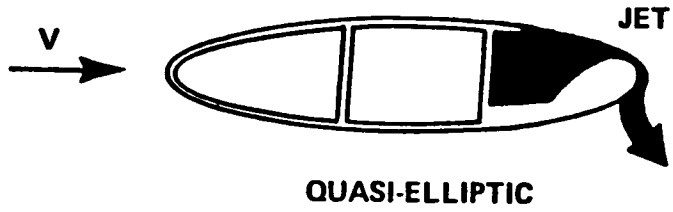

Figure 1. - Circulation control airfoil.

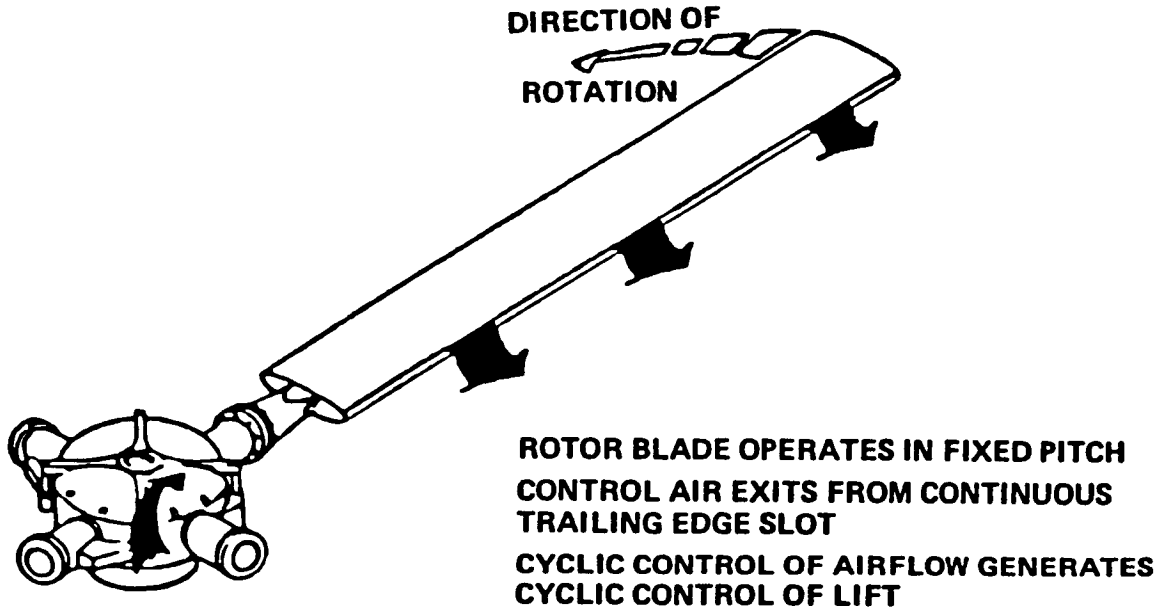

Figure 2. - Circulation control rotor concept.

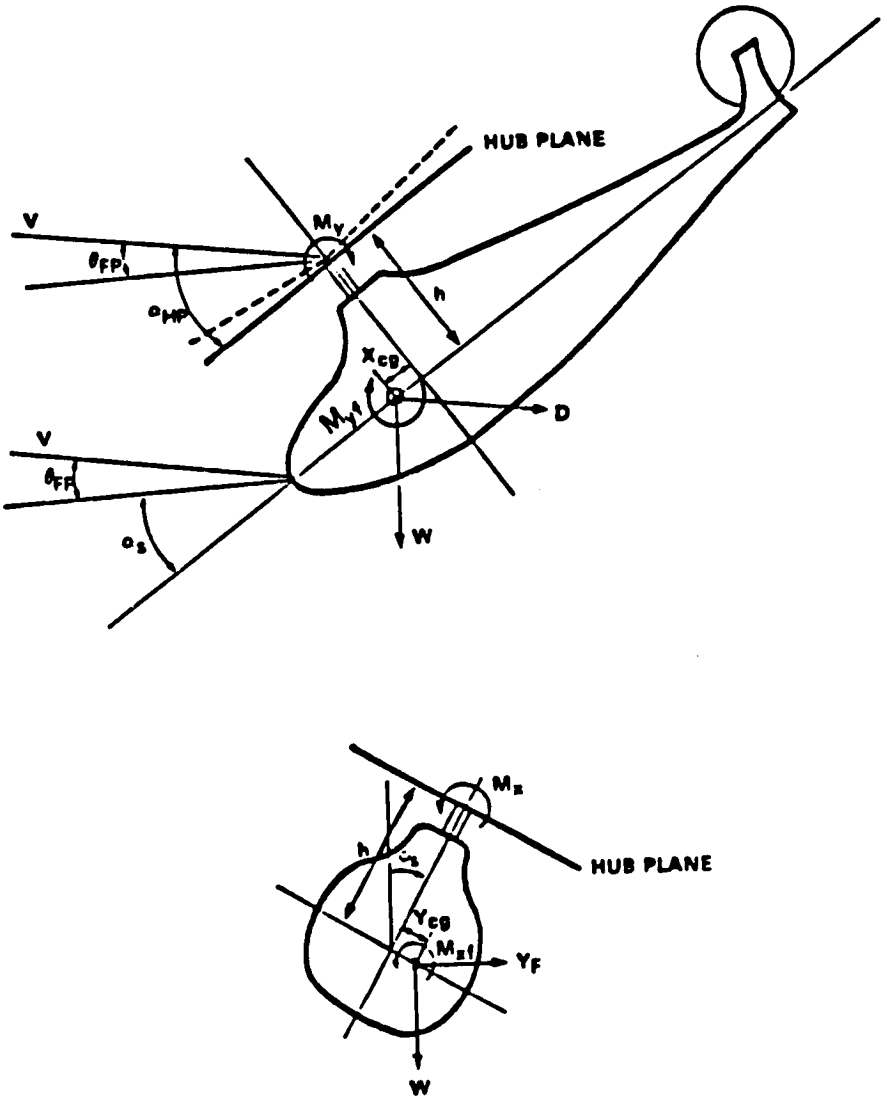

Figure 3. - Vehicle trim configurations.

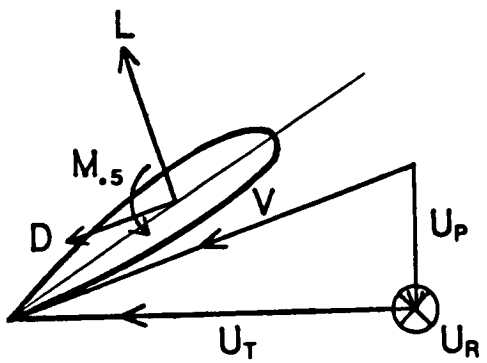

Figure 4. - Blade-section aerodynamics.

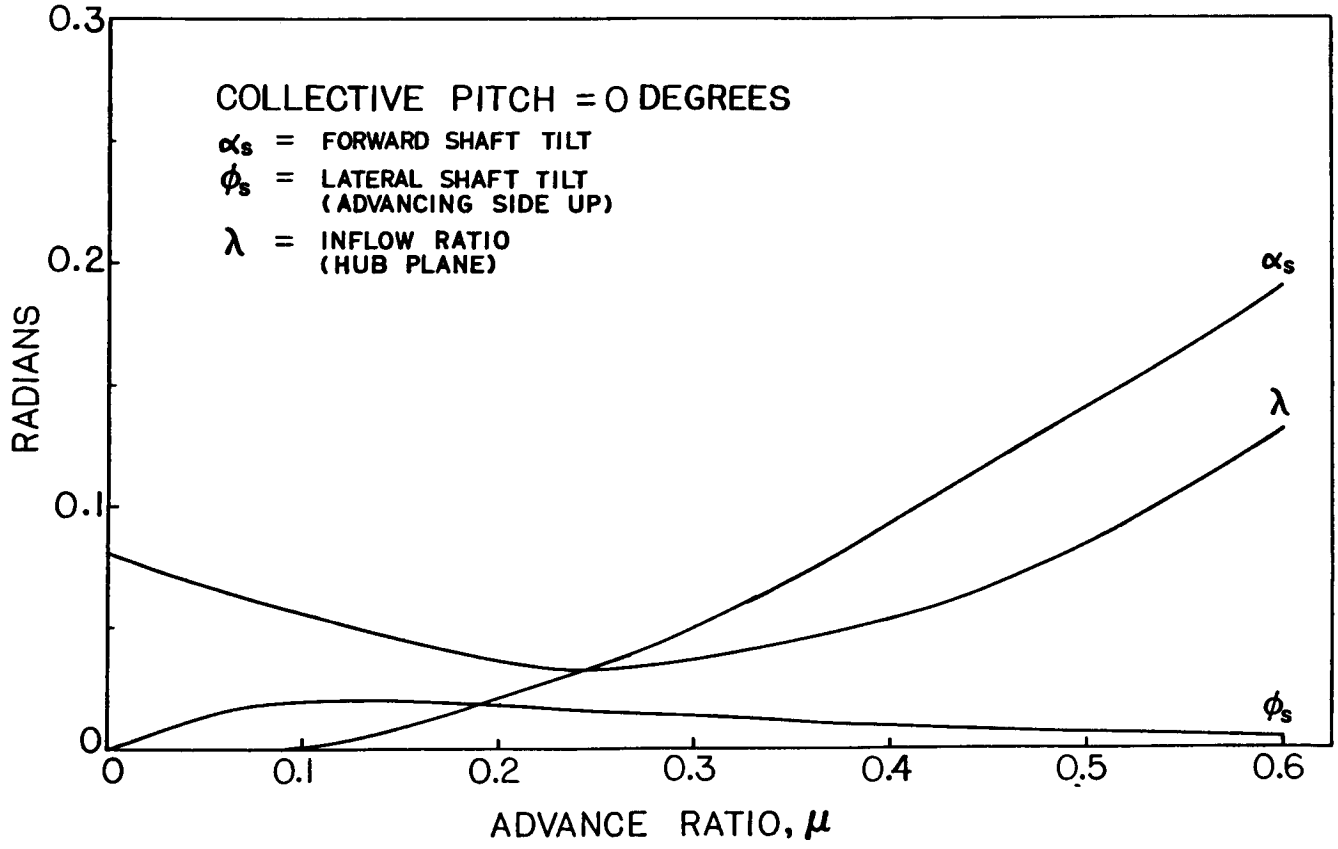

(a) Rotor altitude and mean inflow.

Figure 5. - Vehicle propulsive trim solutions for a collective pitch of zero degree ($C_T/\sigma = 0.1$, $\nu_\beta = 2.3$, $\nu_\zeta = 2.6$, $\nu_\theta = 18$)

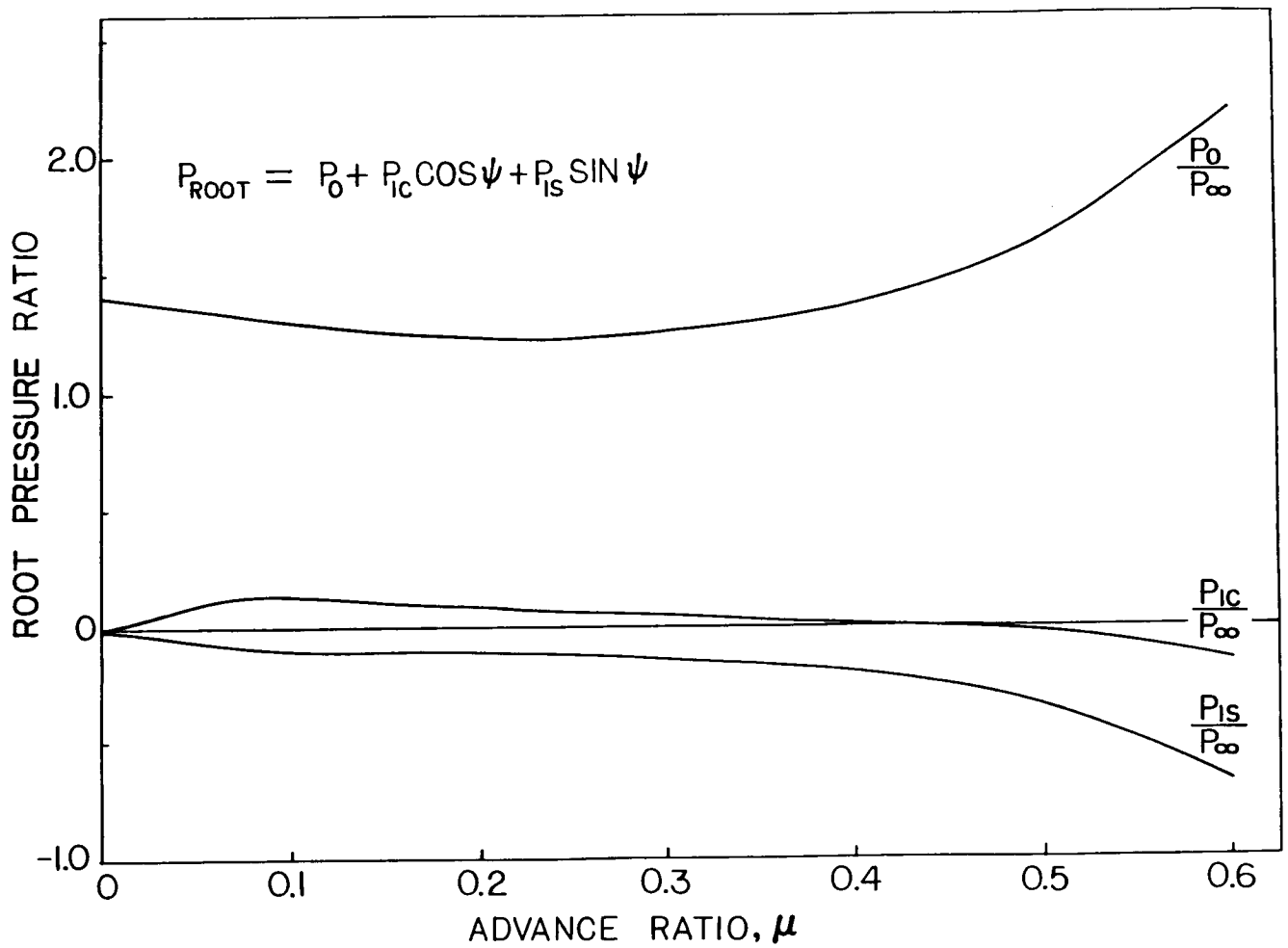

(b) Blowing pressure requirements for trim.

Figure 5.- Continued.

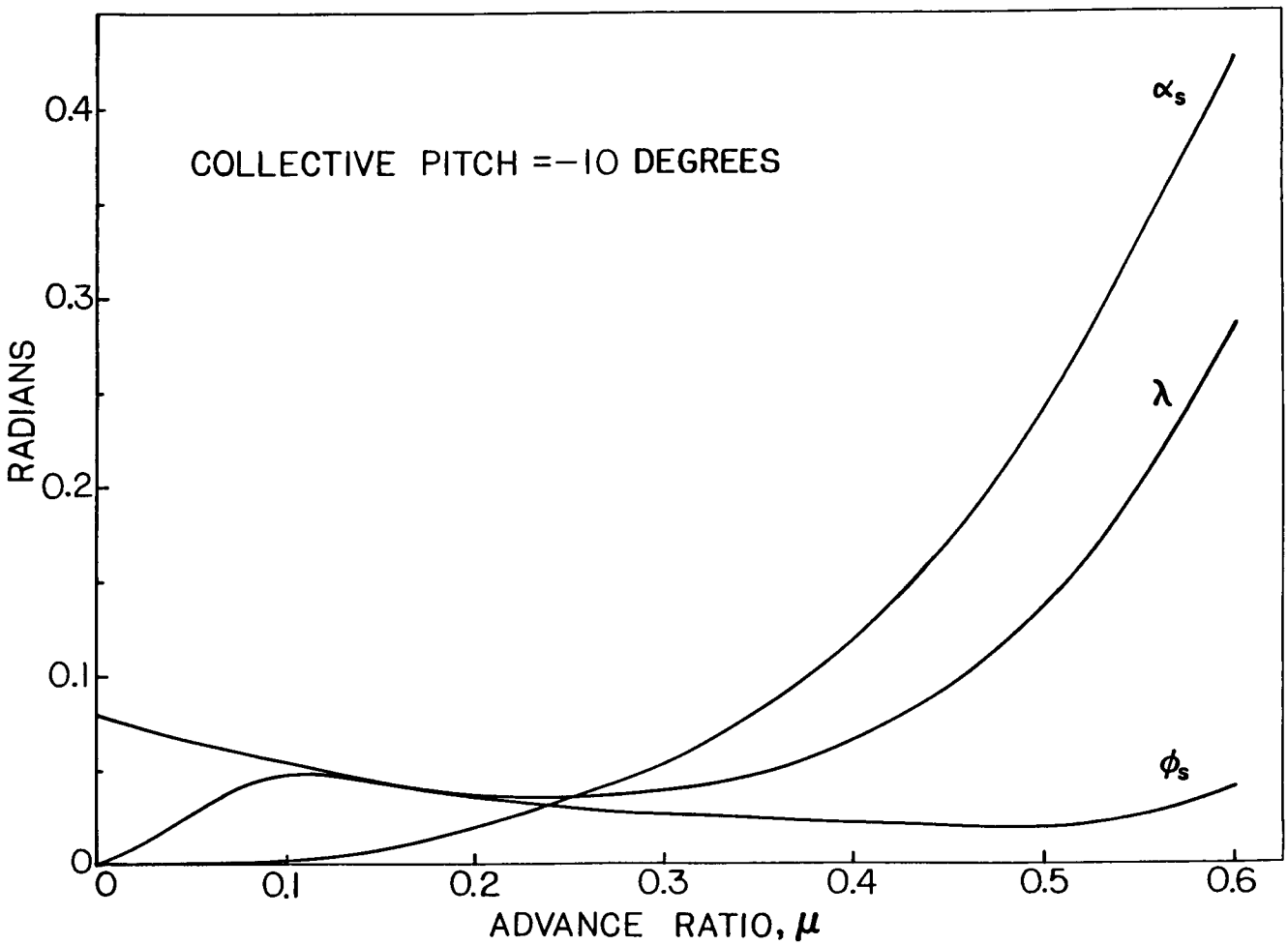

(a) Rotor altitude and mean inflow.

Figure 6. - Vehicle propulsive trim solutions for a collective pitch of -10 degrees. ($C_T/\sigma = 0.1$, $\nu_\beta = 2.3$, $\nu_\zeta = 2.6$, $\nu_\theta = 18$)

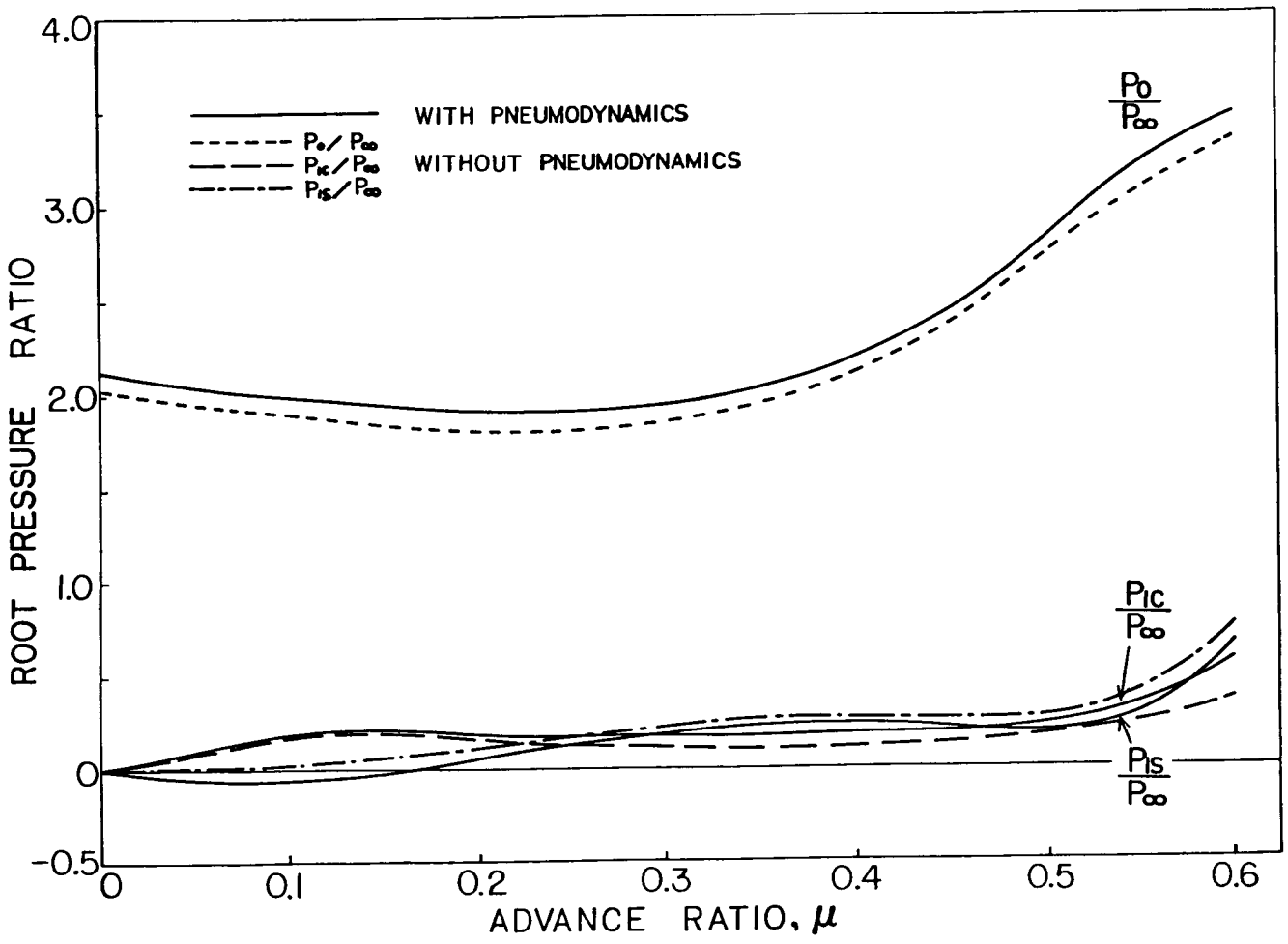

(b) Blowing pressure requirements for trim.

Figure 6.- Concluded.

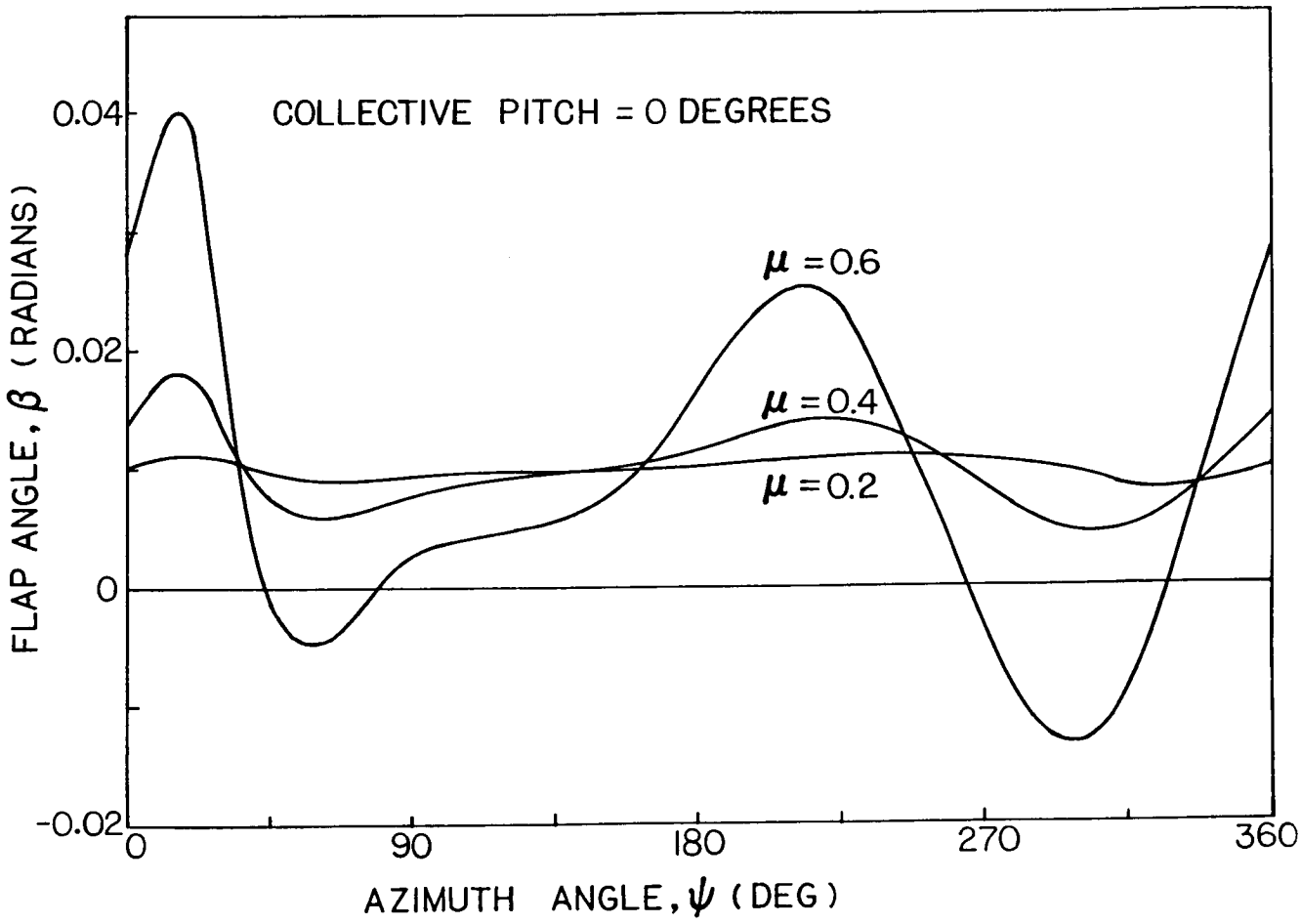

Figure 7. - Blade flap responses for various advance ratios. (C_T/σ = 0.1, ν_β = 2.3, ν_ζ = 2.6, ν_θ = 18)

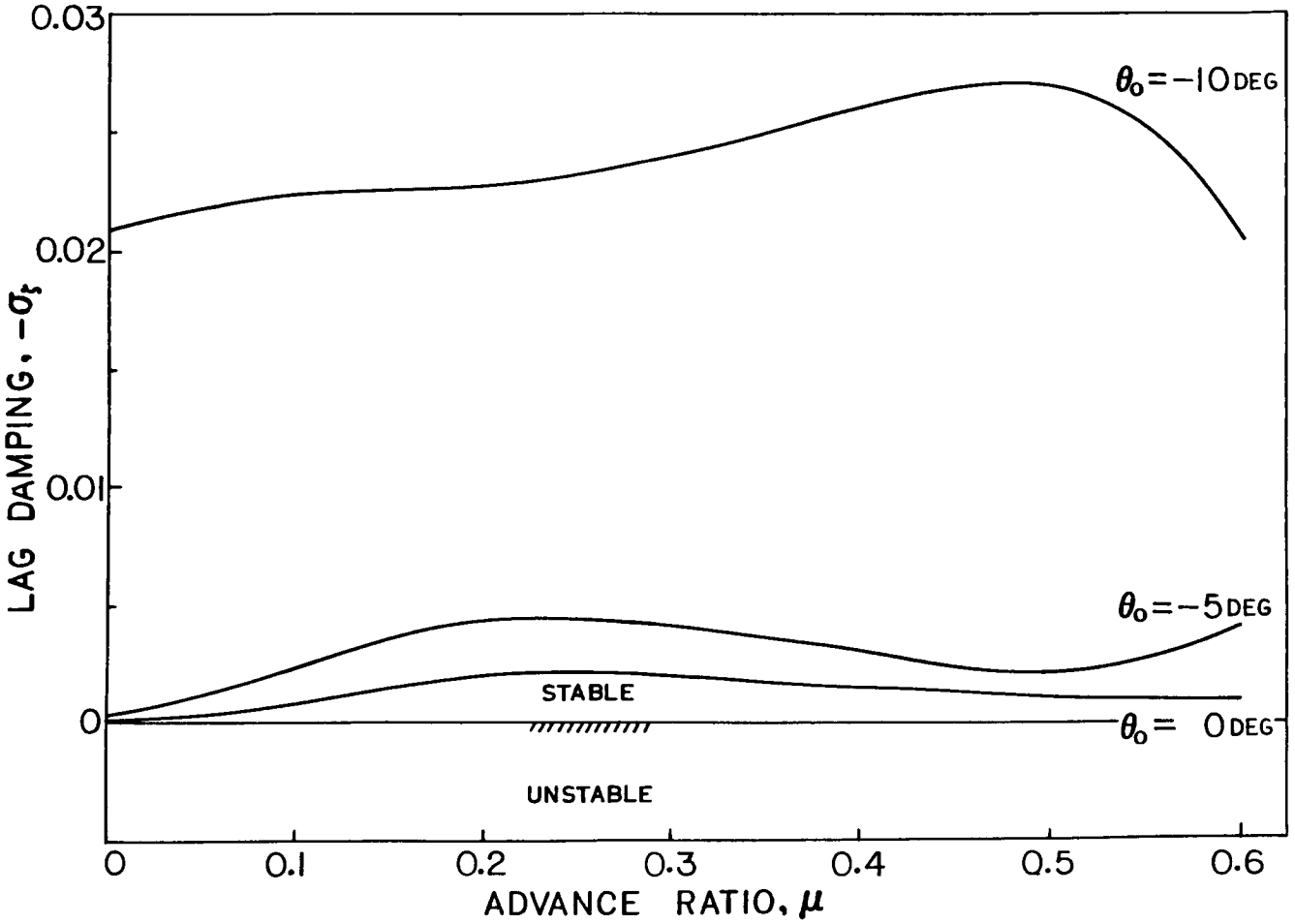

Figure 8. - Effect of collective pitch on low frequency cyclic lag mode. ($C_T/\sigma = 0.1$, $\nu_\beta = 2.3$, $\nu_\zeta = 2.6$, $\nu_\theta = 18$)

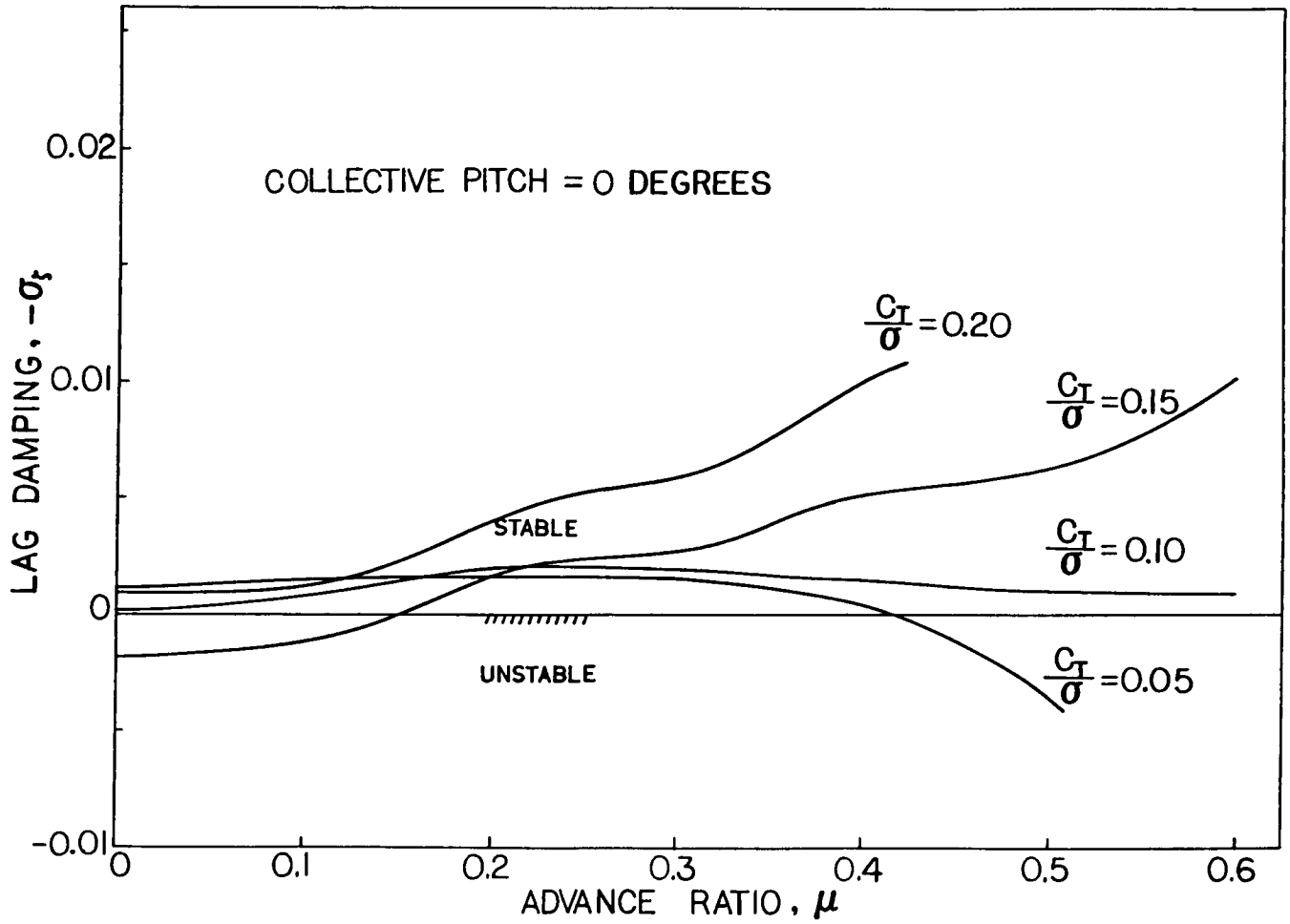

Figure 9. - Effect of thrust level on low frequency cyclic lag mode. (ν_β = 2.3, υ_ζ = 2.6, υ_θ)

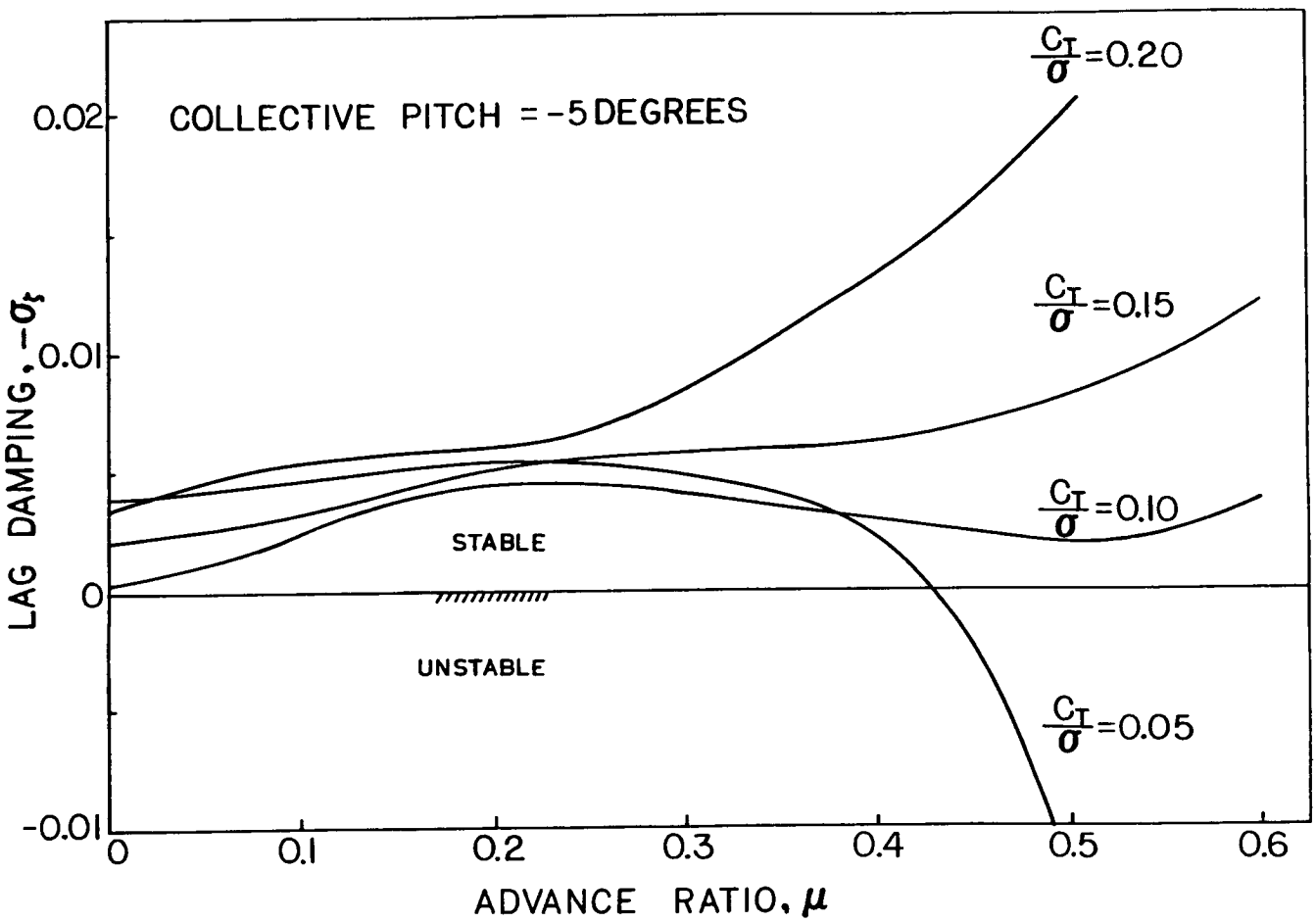

Figure 10. - Effect of thrust level on low frequency cyclic lag mode. ($\nu_\beta = 2.3$, $\nu_\zeta = \nu_\theta = 18$)

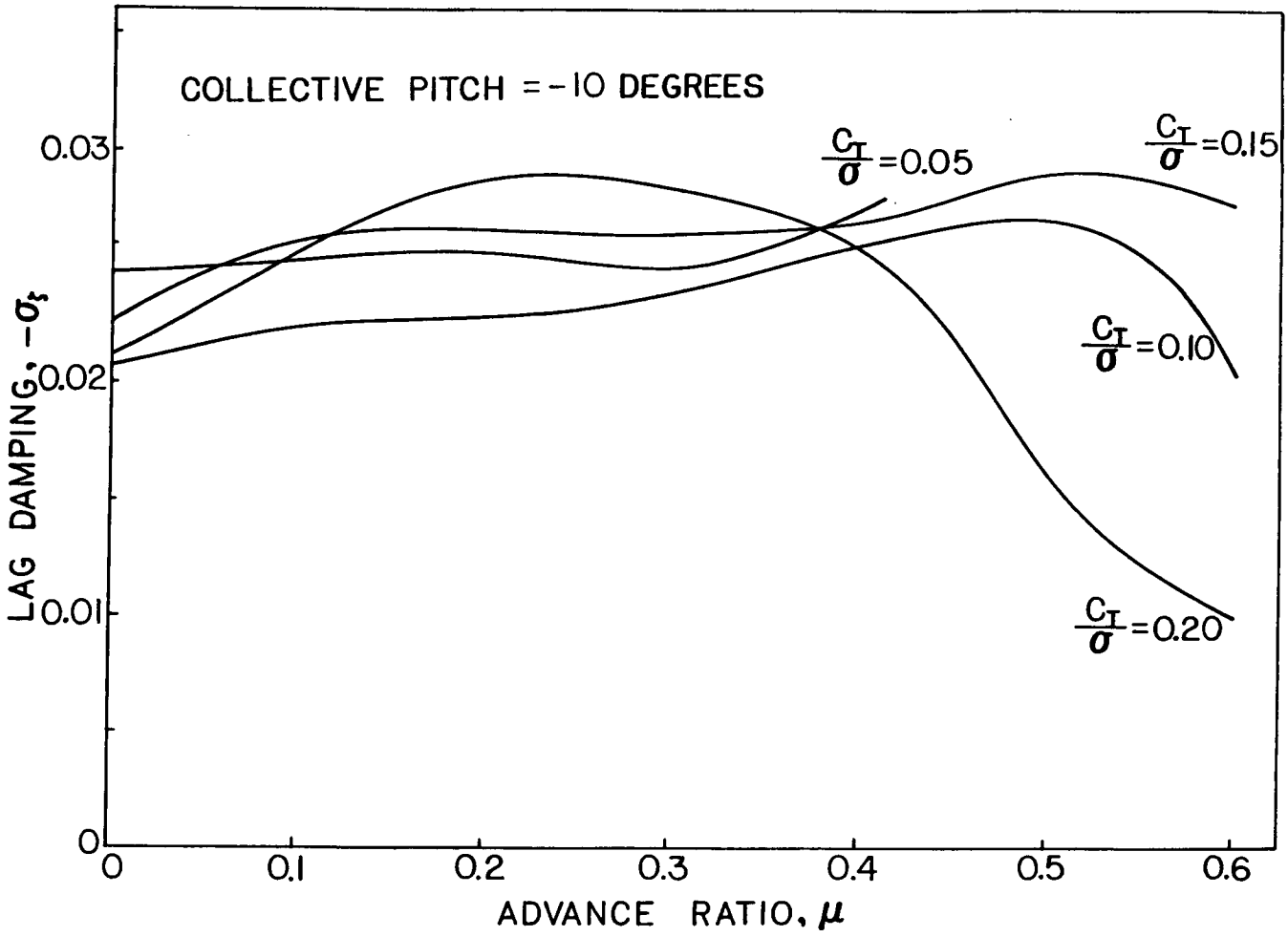

Figure 11. - Effect of thrust level on low frequency cyclic lag mode. (ν_β = 2.3, $\nu_\zeta = \nu_\theta$ = 18)

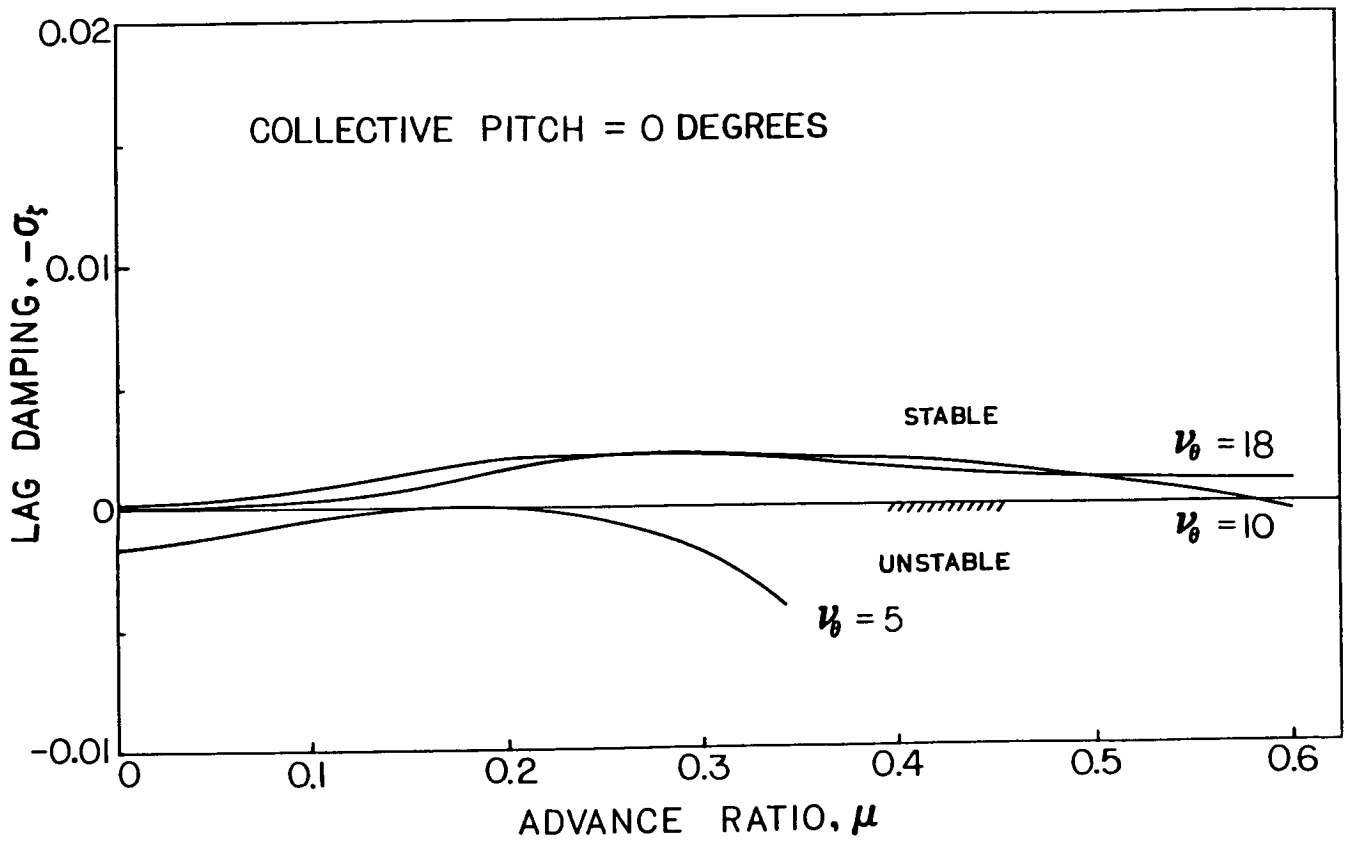

(a) Collective pitch = 0 degrees.

Figure 12. - Effect of torsional stiffness on low frequency cyclic lag mode. ($C_T/\sigma = 0.1$, $\nu_\beta = 2.3$, $\nu_\zeta = 2.6$)

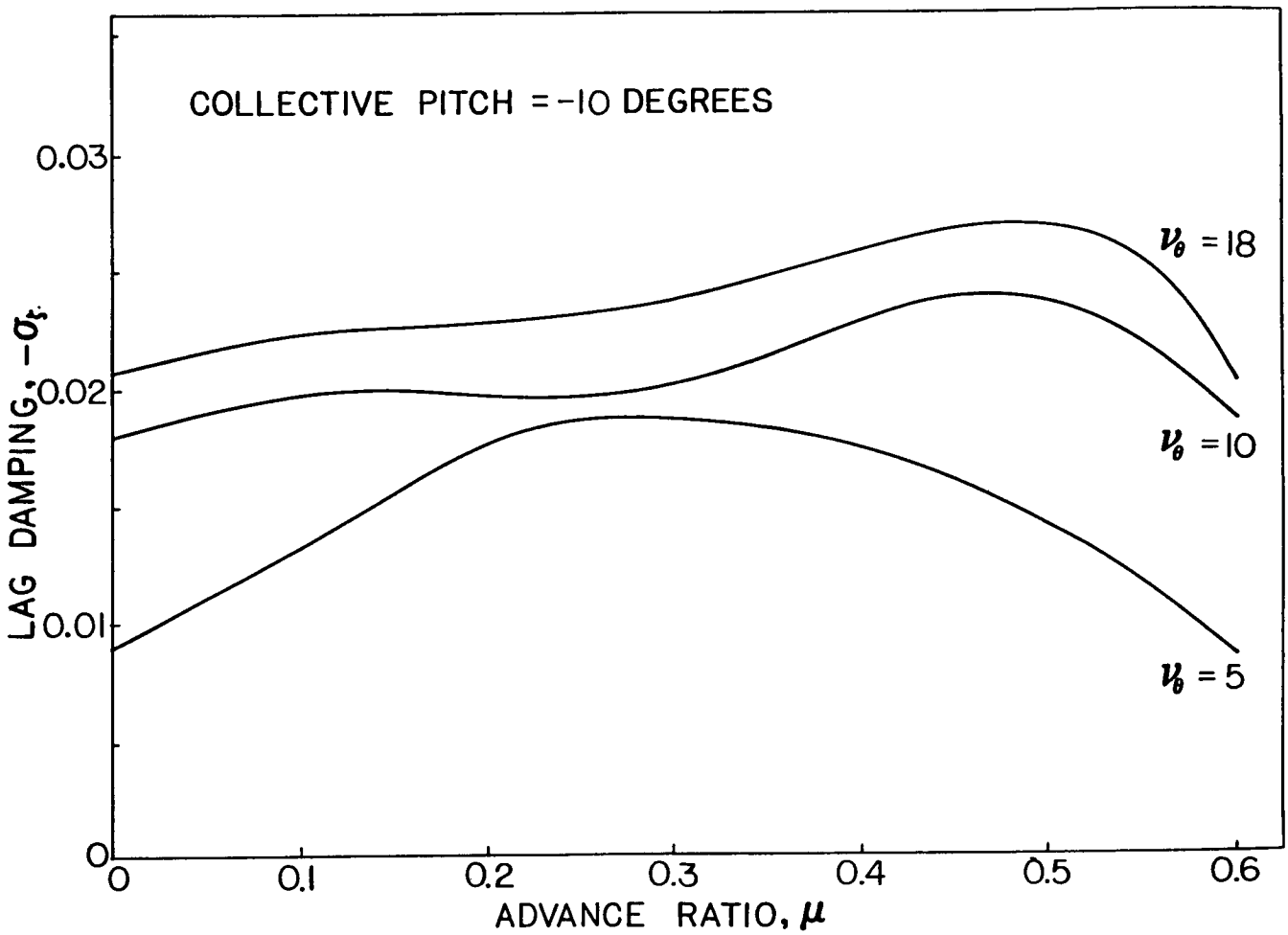

(b) Collective pitch -10 degrees.

Figure 12.- Concluded.

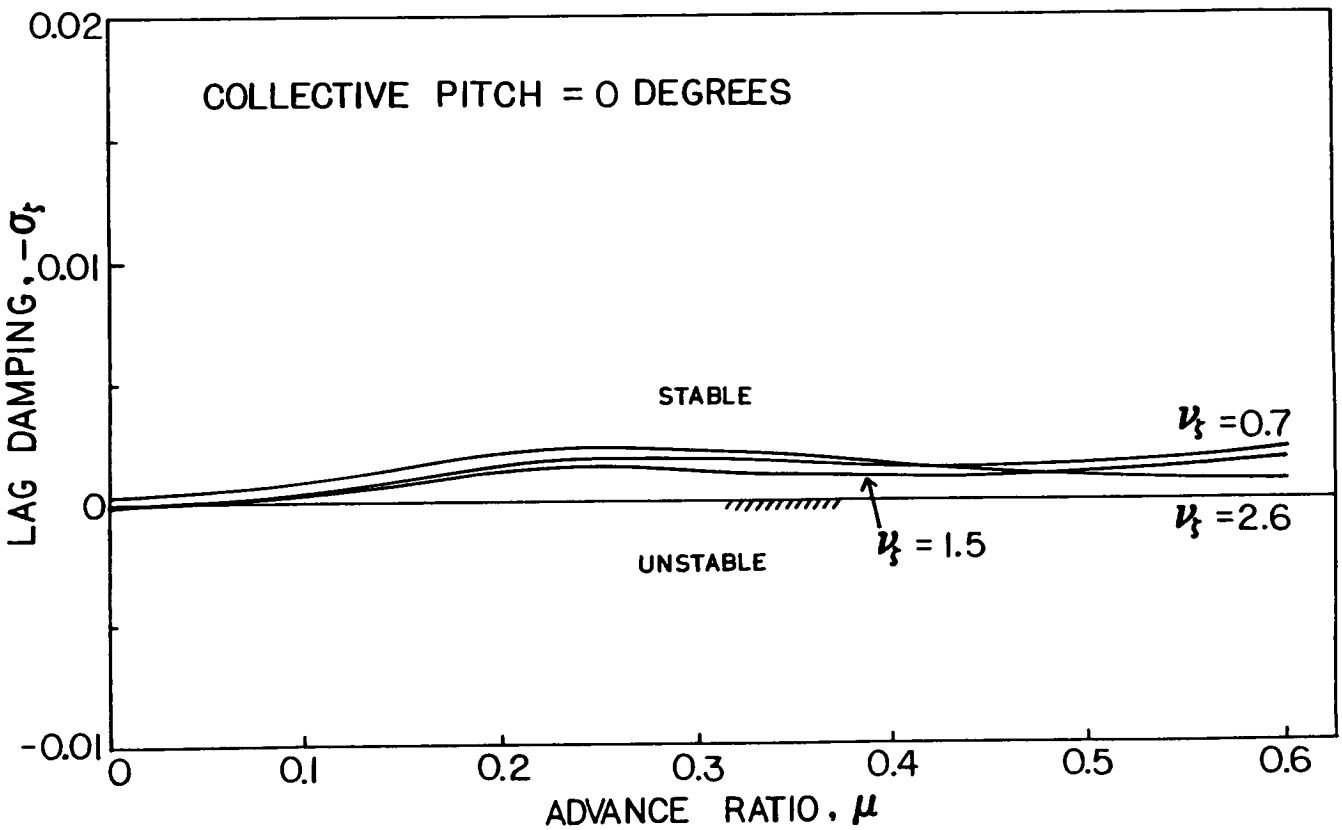

(a) Collective pitch = 0 degrees.

Figure 13. - Effect of lag stiffness on low frequency cyclic lag mode. (C_T/σ = 0.1, ν_β = 2.3, ν_θ = 18)

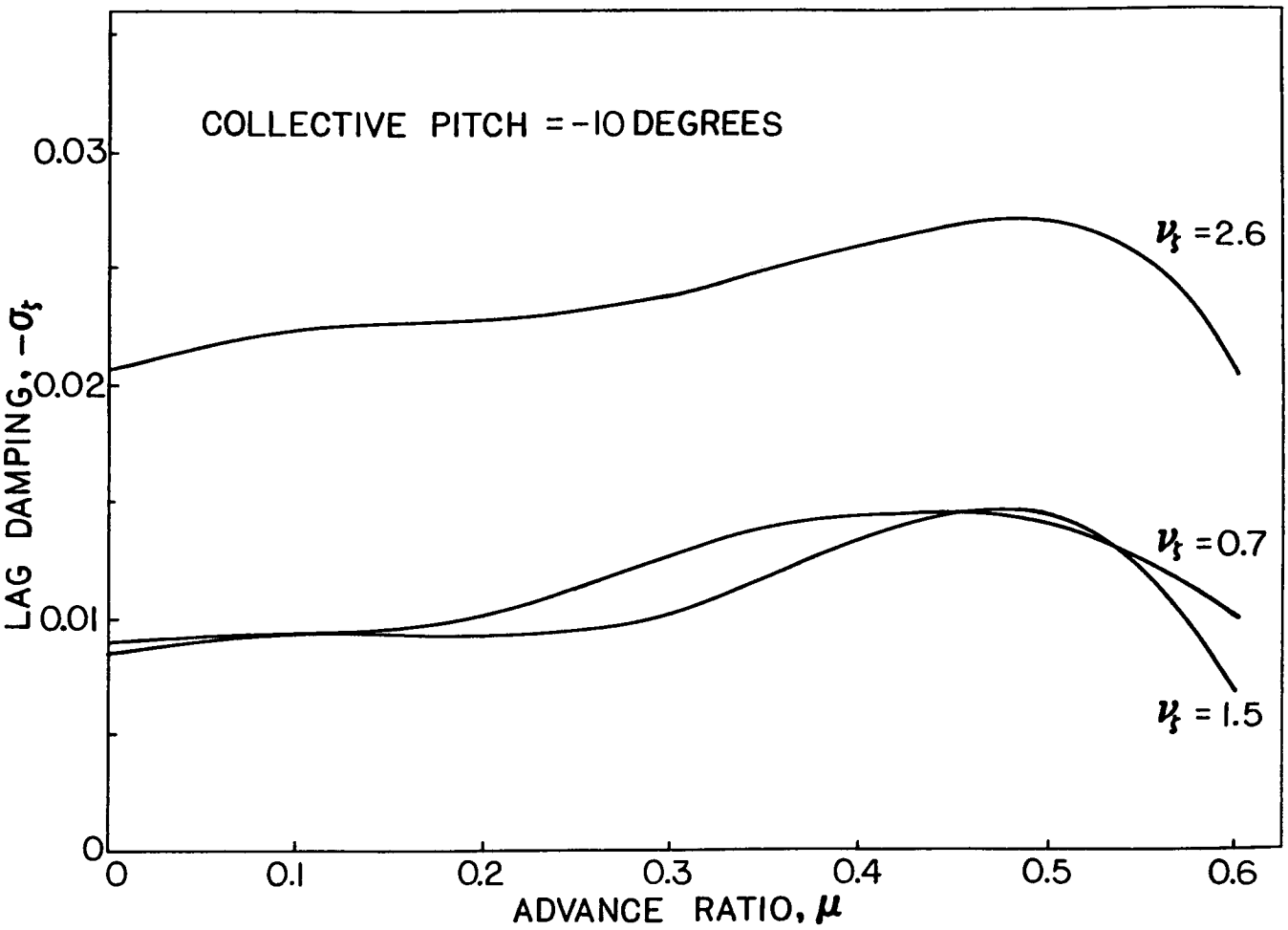

(b) Collective pitch -10 degrees.

Figure 13.- Concluded.

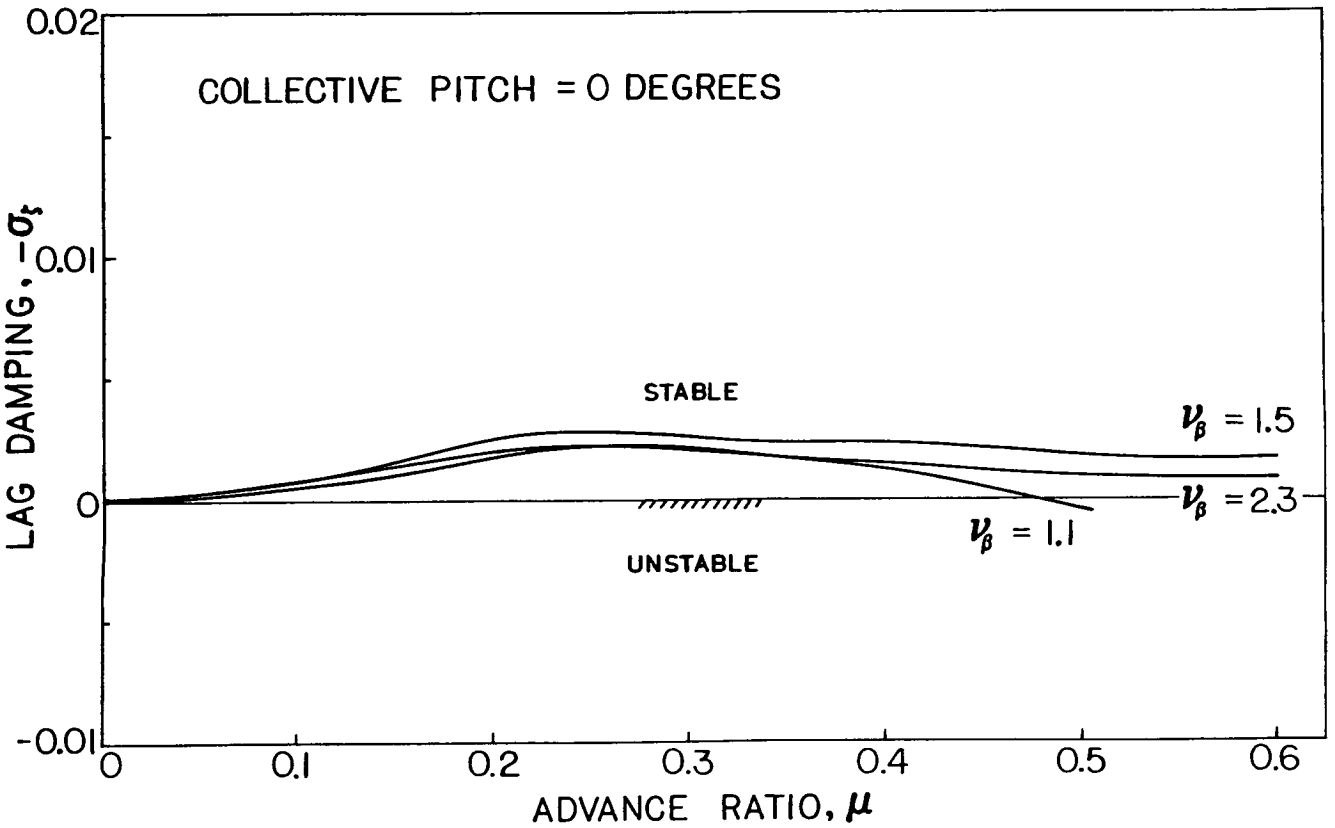

(a) Collective pitch = 0 degrees.

Figure 14. - Effect of flap stiffness on low frequency cyclic lag mode. (C_T/σ = 0.1, ν_ζ = 2.6, ν_θ = 18)

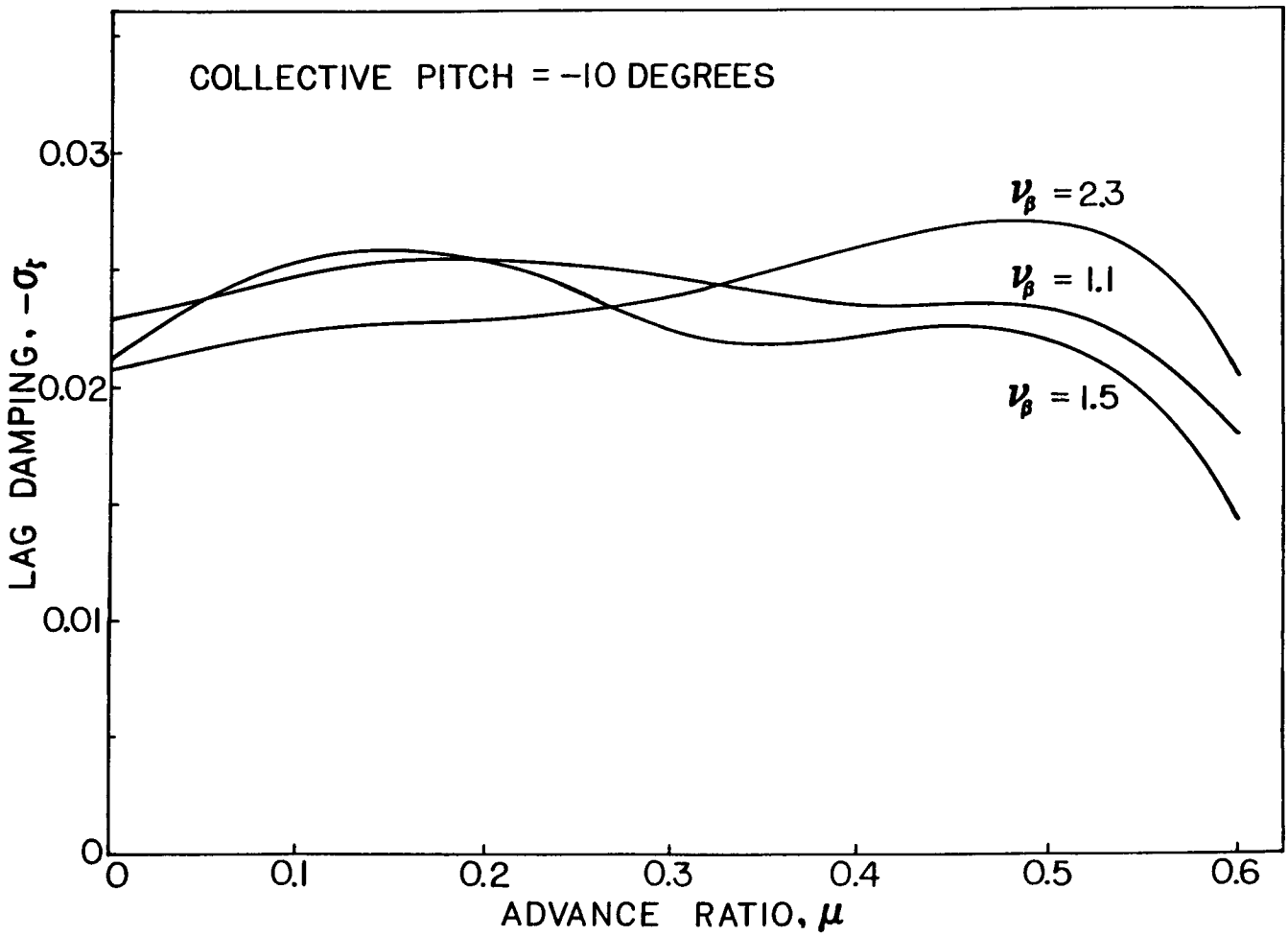

(b) Collective pitch -10 degrees.

Figure 14.- Concluded.

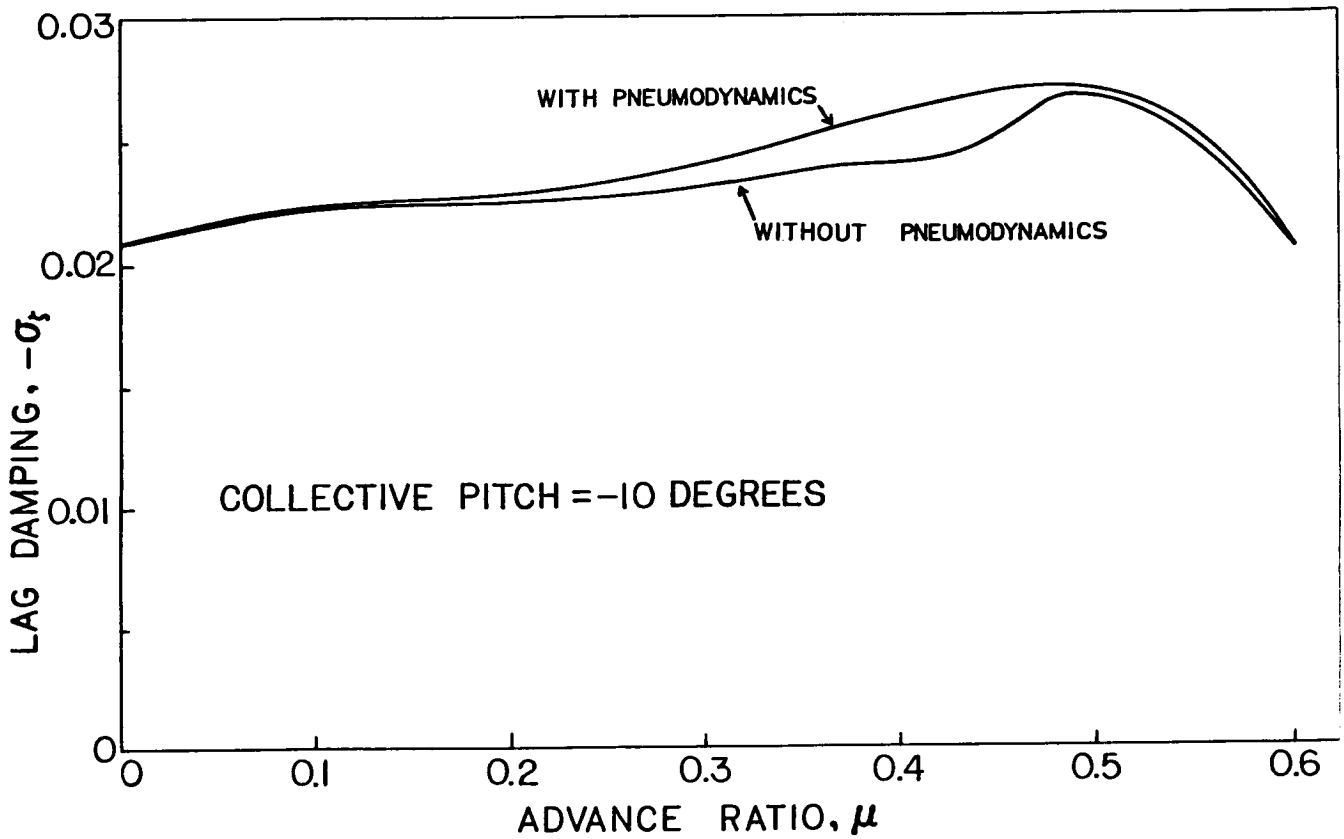

Figure 15. - Effect of pneumodynamics on low frequency cyclic lag mode. ($C_T/\sigma = 0.1$, $\nu_\beta = 2.3$, $\nu_\zeta = 2.6$, $\nu_\theta = 18$)

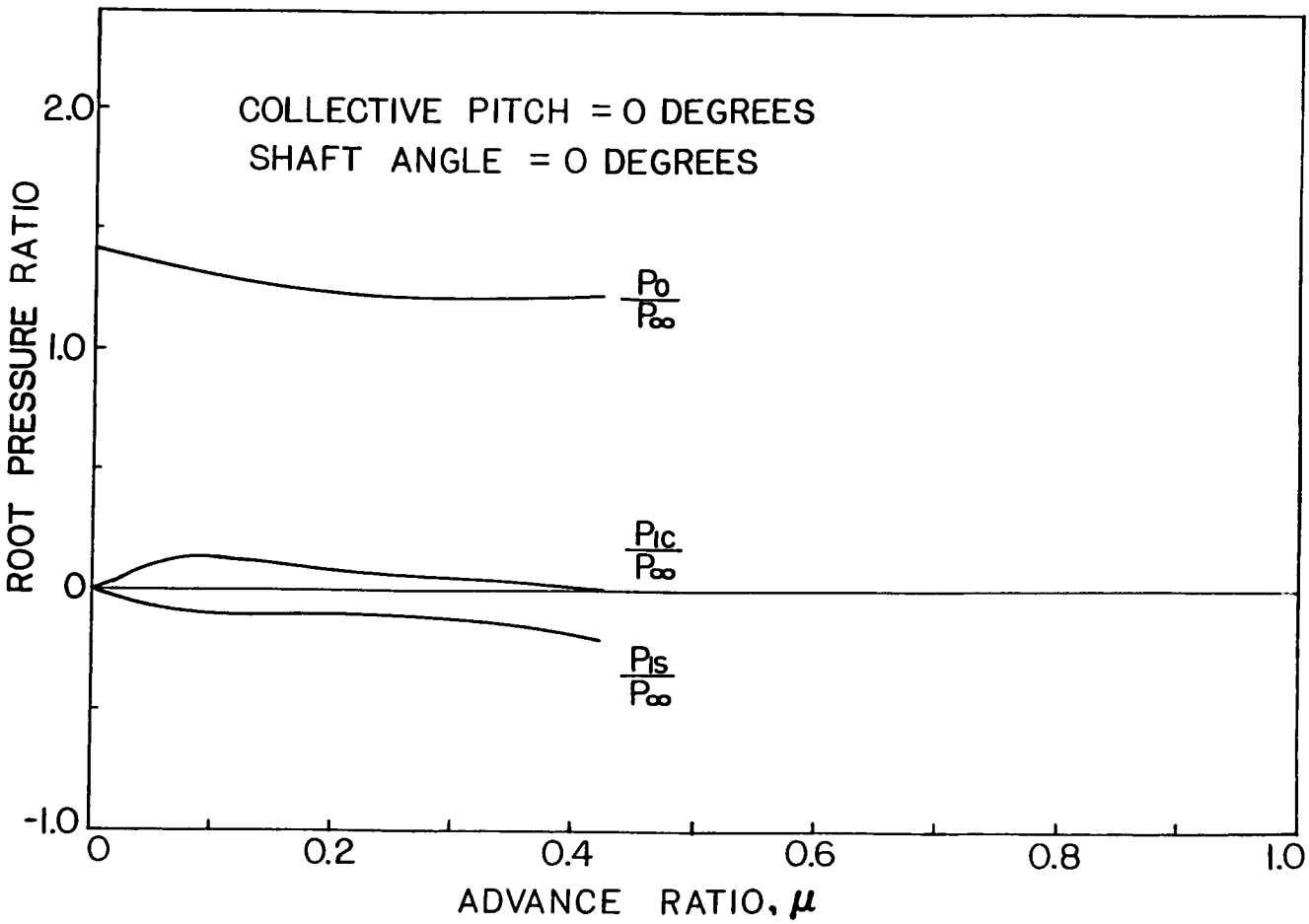

Figure 16. - Blade root blowing pressure requirements for the constrained trim solution. ($C_T/\sigma = 0.1$, $\nu_\beta = 2.3$, $\nu_\zeta = 2.6$, $\nu_\theta = 18$)

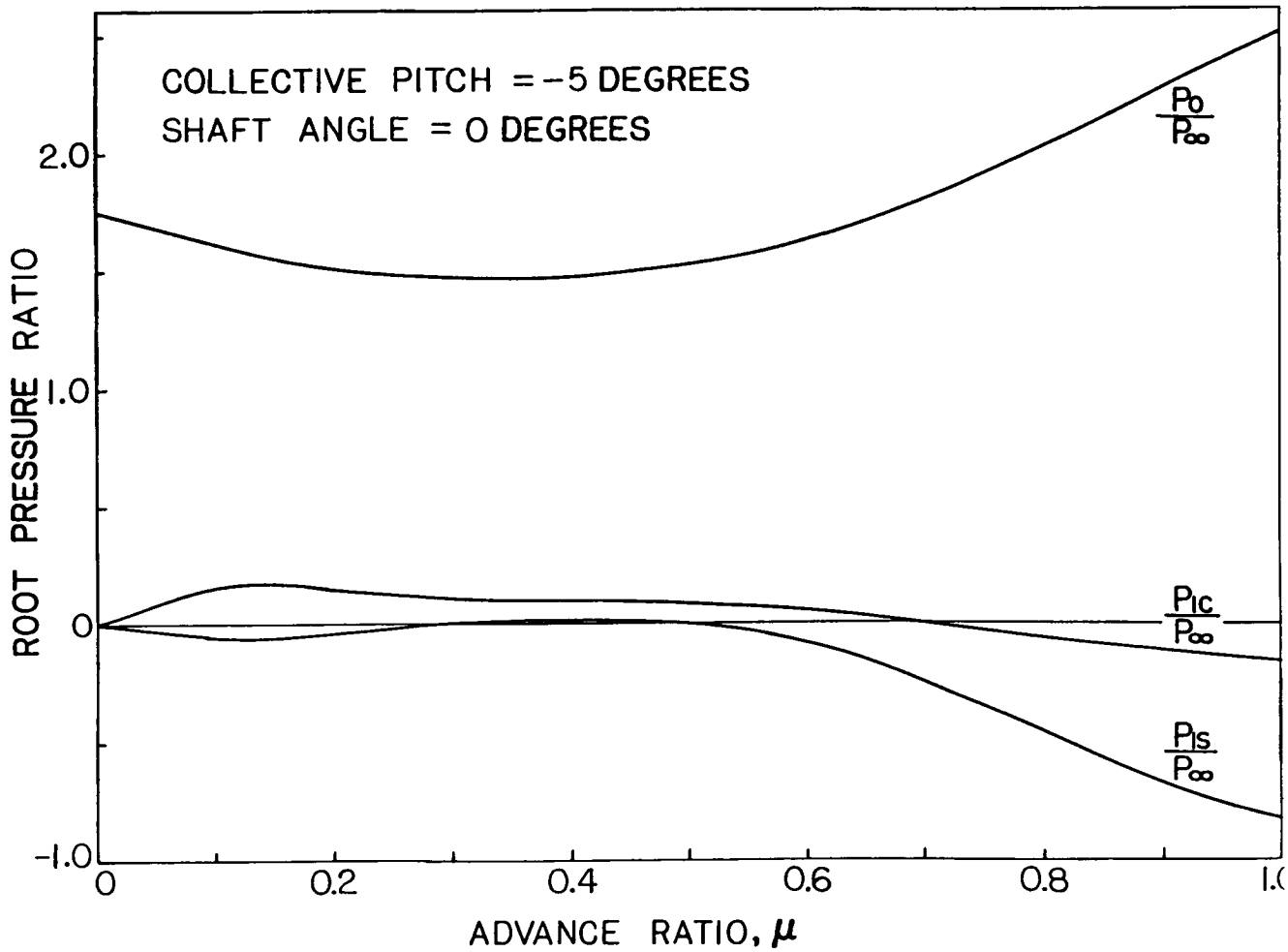

Figure 17. - Blade root blowing pressure requirements for the constrained trim solution. ($C_T/\sigma = 0.1$, $\nu_\beta = 2.3$, $\nu_\zeta = 2.6$, $\nu_\theta = 18$)

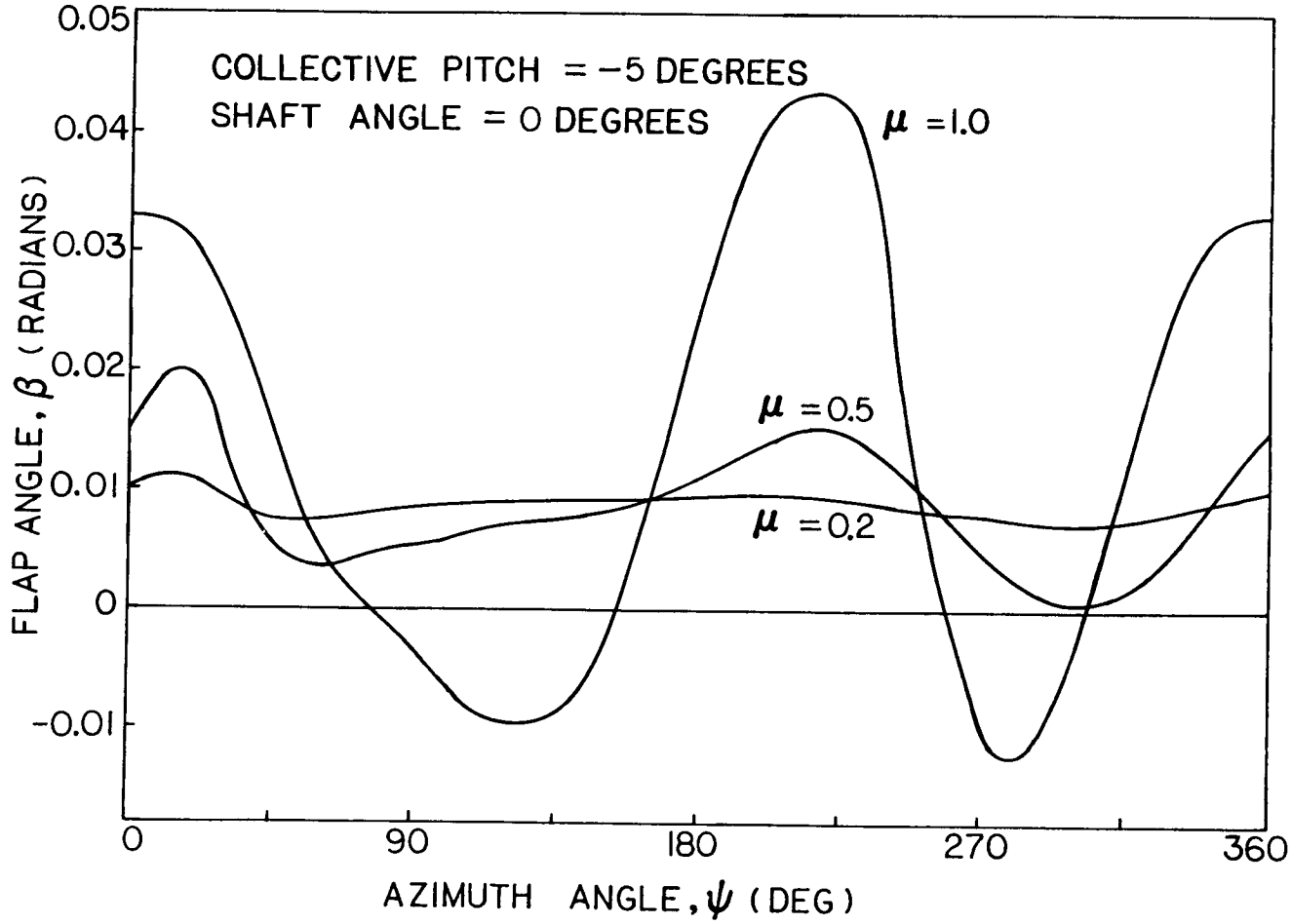

Figure 18. - Blade flap response for various advance ratios. (C_T/σ = 0.1, ν_β = 2.3, ν_ζ = 2.6, ν_θ = 18)

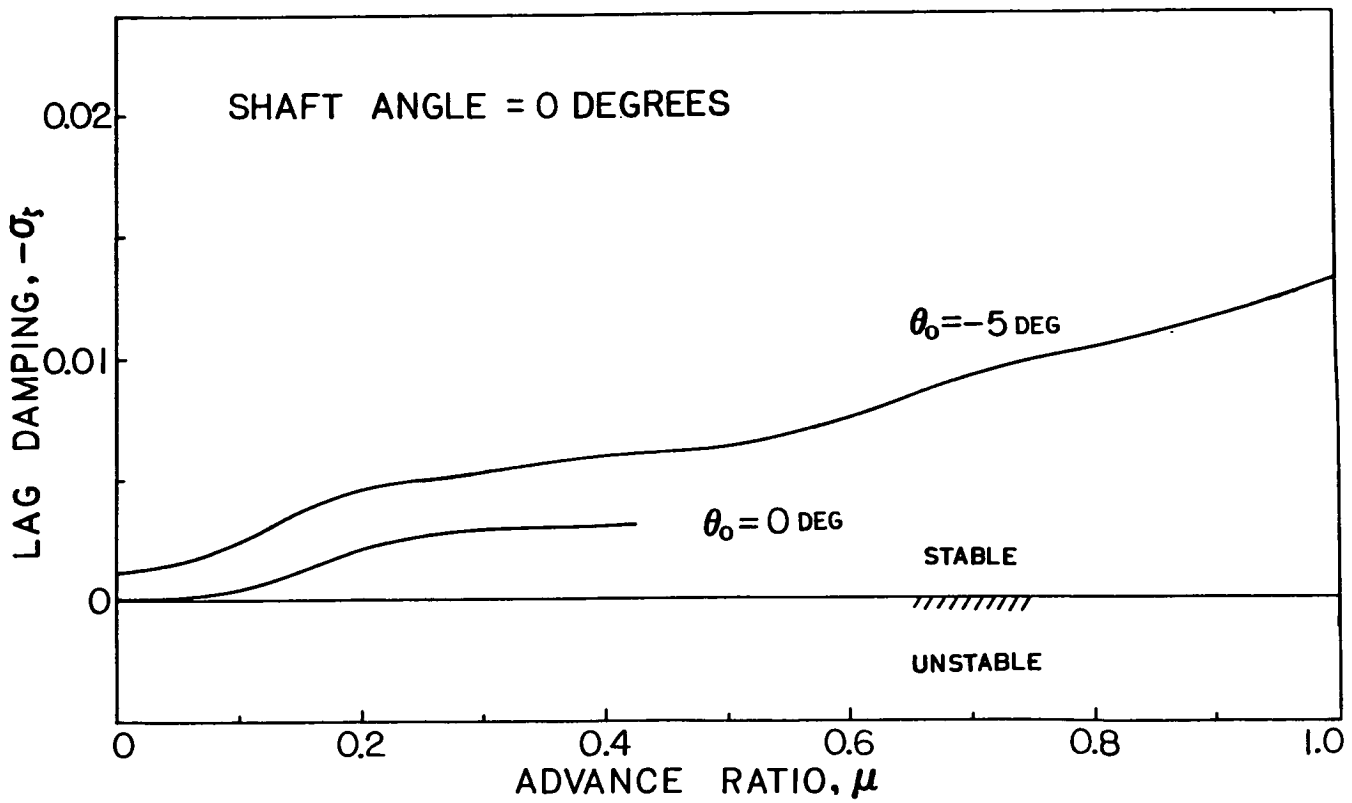

Figure 19. - Effect of collective pitch on low frequency cyclic lag mode. (C_T/σ = 0.1, ν_β = 2.3, ν_ζ = 2.6, ν_θ = 18)

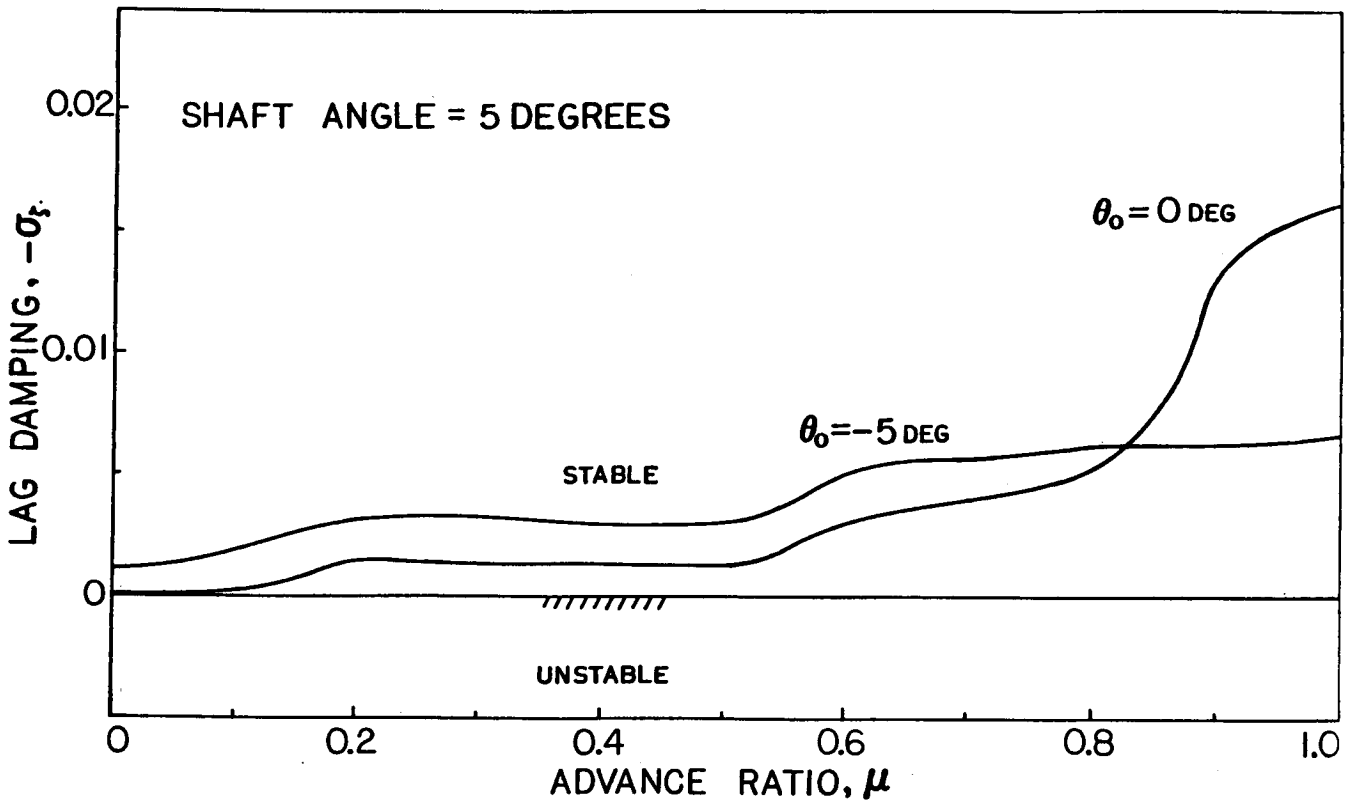

Figure 20. - Effect of collective pitch on low frequency cyclic lag mode. ($C_T/\sigma = 0.1$, $\nu_\beta = 2.3$, $\nu_\zeta = 2.6$, $\nu_\theta = 18$)

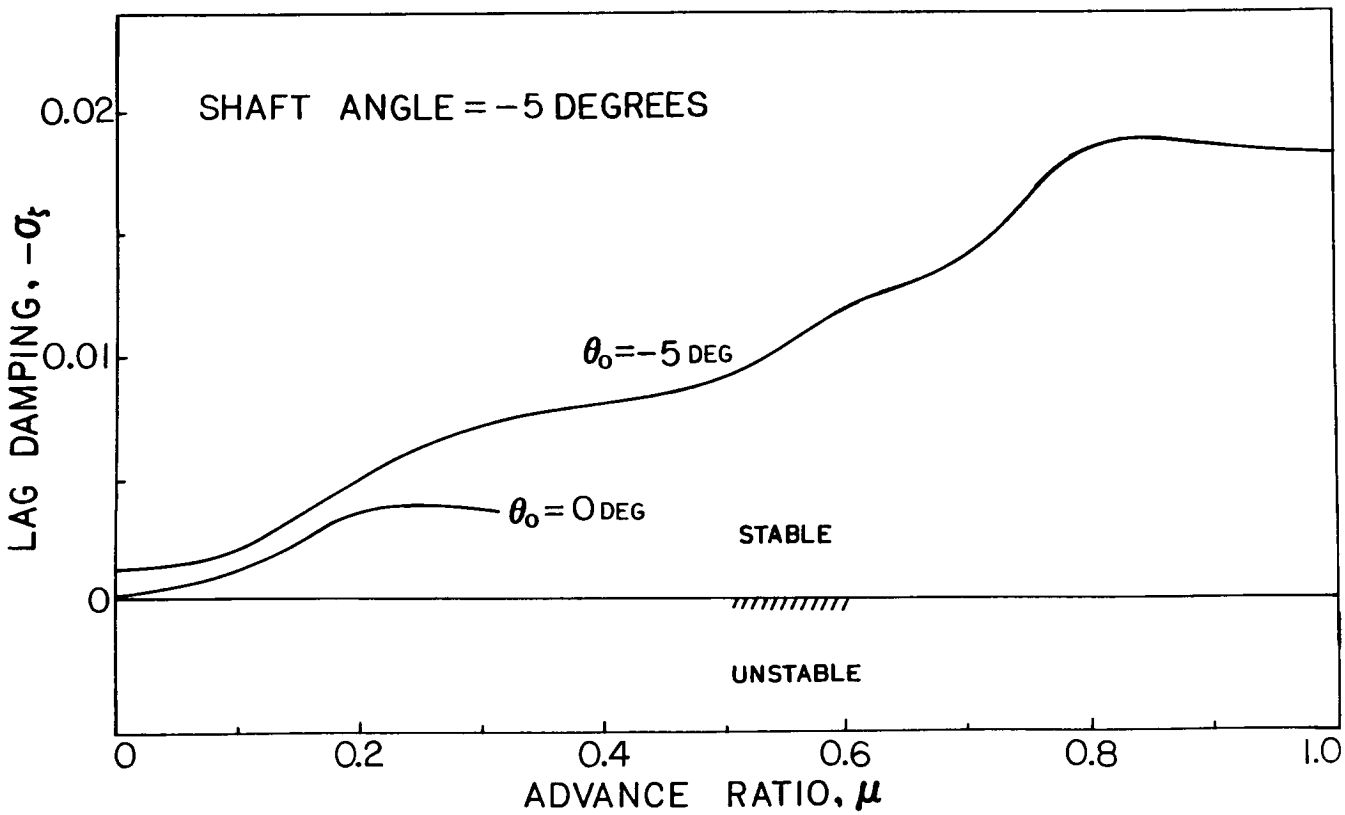

Figure 21. - Effect of collective pitch on low frequency cyclic lag mode. (C_T/σ = 0.1, ν_β = 2.3, ν_ζ = 2.6, ν_θ = 18)